Aging and Disease
www.aginganddisease.org
Early access date: December 15, 2025
http://dx.doi.org/10.14336/AD.2025.1122

Original Article

Hv1 Upregulation Worsens Spinal, Spleen, and Lung Molecular Pathology and Impairs Locomotion after Spinal Cord Injury in Aged Male Mice

Zihui Wang[1#], Yun Li[1#], Hangnoh Lee[2], Zhuofan Lei[1], Long-Jun Wu[3], Junfang Wu[1*]

[1]Department of Anesthesiology and Center for Shock, Trauma and Anesthesiology Research (STAR), University of Maryland School of Medicine, Baltimore, MD, USA. [2]Department of Medicine, University of Maryland School of Medicine, Baltimore, MD, USA. [3]Center for Neuroimmunology and Glial Biology, Institute of Molecular Medicine, University of Texas Health Science Center at Houston, Houston, TX, USA.

[Received September 3, 2025; Revised December 11, 2025; Accepted December 13, 2025]

ABSTRACT: Spinal cord injury (SCI) causes not only intraspinal damage but also systemic organ pathology, with aging as a key determinant of outcomes. The mechanisms by which old age aggravate SCI pathology remain unclear. The voltage-gated proton channel Hv1 plays a key role in regulating immune responses. Hv1 increases with aging and SCI, and Hv1 KO provides neuroprotection in young mice. We hypothesized that age-related Hv1 upregulation worsens spinal cord, spleen, and lung pathology and hinders locomotor recovery after SCI via immune modulation. Using aged Hv1 KO and WT male mice subjected to moderate SCI, we assessed behavioral and molecular outcomes. Transcriptomic analysis revealed that Hv1 mRNA expression was higher in the brains of aged sham mice and further upregulated in injured spinal cord tissues. Spinal cord RNA-seq showed acute innate immune and cytokine activation in both genotypes. Hv1 deletion enhanced chromatin remodeling, epigenetic and Wnt signaling, while suppressing NF-κB-driven inflammation and oxidative stress–induced apoptosis. In the spleen, Hv1 depletion enhanced immune responses while suppressing mitosis. T cell and leukocyte activation increased, whereas lung cytokine signaling decreased. Functional recovery improved with reduced tissue damage. After chronic SCI, Hv1 KO mice showed elevated circadian rhythm and T cell proliferation in the spinal cord, increased mitotic gene expression but reduced adaptive immunity in the spleen, and enhanced immune activation with decreased cilium activity in the lungs. Together, our findings reveal how Hv1 contributes to age-related intraspinal damage and peripheral immune dysfunction after SCI, highlighting a potential therapeutic target for elderly patients.

Keywords: Old age, spinal cord injury, Hv1, bulk RNA sequencing, behavioral function

INTRODUCTION

Traumatic spinal cord injury (SCI) represents a severe neurological disorder characterized by chronic motor and sensory impairments and secondary complications, which together substantially compromise quality of life [1]. With the significant demographic shifts [2], aging has emerged as a critical determinant in SCI with a notable increase in the proportion of SCI cases [3, 4]. Compared to young patients, age-related muscle and bone disorders increase the risk of falls and trauma in elderly individuals [5], leading to higher complication rates and poorer neurological recovery. Clinical studies have shown that older age at injury is significantly associated with poorer neurological and functional recovery [6-8], as well as increased mobility and mortality risk [9, 10]. In rodent models, age worsens functional recovery after SCI, which has been consistently observed across laboratories in both mice and rats [11-15]. In addition, aging significantly increases the susceptibility to severe complications after

***Correspondence should be addressed to:** Dr. Junfang Wu, University of Maryland School of Medicine, Baltimore, MD, USA. Email: junfang.wu@som.umaryland.edu.

SCI, including impaired wound healing, heightened inflammatory responses, and reduced functional recovery [16]. Individuals over the age of 61 demonstrated a higher incidence of post-injury complications, including pneumonia, gastrointestinal hemorrhage, pulmonary embolism, and renal dysfunction [16]. These age-dependent differences underscore the urgent need to identify molecular mechanisms that worsen SCI outcomes in older individuals.

Beyond direct spinal cord damage, SCI induces widespread systemic effects that contribute to disease progression. Injury disrupts immune homeostasis, leading to splenic atrophy, impaired lymphocyte function, and increased vulnerability to infections such as pneumonia [17-20]. Pulmonary complications are a leading cause of death in SCI patients, particularly in older adults [21-25]. The systemic nature of these complications suggests that pathological processes extend beyond the spinal cord and involve maladaptive interactions between central and peripheral organs. However, the molecular mediators that link central injury responses with peripheral immune and pulmonary dysfunction remain incompletely defined, especially in the context of aging.

The voltage-gated proton channel Hv1, encoded by *Hvcn1*, is highly expressed in microglia, macrophages, and other immune cells, where it sustains NADPH oxidase activity and drives production of reactive oxygen species (ROS) [26-28]. While physiological ROS levels are essential for host defense, excessive Hv1-dependent ROS generation amplifies oxidative stress and proinflammatory signaling. Experimental evidence has implicated Hv1 in ischemic stroke, multiple sclerosis, and neurodegeneration, where Hv1 promotes microglial activation and worsens neurological damage [29-33]. While Hv1 upregulation is known to exacerbate secondary damage after traumatic CNS injuries by promoting ROS and neuroinflammation [34-41], its role in age-dependent pathology remains unclear. Importantly, Hv1 expression and activity increase with age [42, 43], raising the possibility that Hv1 upregulation contributes to age-related susceptibility to injury. Despite this evidence, the role of Hv1 in SCI, particularly in the aged spinal cord and peripheral organs, remains largely unexplored.

Given that SCI elicits robust neuroinflammation in the spinal cord and profound immune dysregulation in the spleen and lungs, Hv1 may act as a common molecular amplifier of central and systemic pathology in aged individuals. In the present study, we investigated the contribution of Hv1 to SCI outcomes in aged male mice. We show that Hv1 upregulation exacerbates molecular pathology in the spinal cord, spleen, and lungs, and leads to impaired locomotor recovery. To our knowledge, this is the first demonstration that Hv1 functions as an age-dependent driver of both central and peripheral pathology after SCI. These findings highlight Hv1 as a promising therapeutic target to improve neurological and systemic outcomes in elderly patients with SCI.

MATERIALS AND METHODS

Mouse Spinal Cord Injury (SCI)

All experimental procedures were carried out in accordance with guidelines approved by the University of Maryland School of Medicine Institutional Animal Care and Use Committee (IACUC). Aged (18-22-month-old) male C57BL/6 mice were sourced from Charles River Laboratories through the National Institute on Aging. Homozygous Hv1 (Hv1 KO) mice breeders [28, 29] were kindly provided by Dr. Long-Jun Wu and maintained in the animal facility at the University of Maryland School of Medicine. All animals were housed in a standard 12 h light/dark cycle with free access to food and water. All mice were randomly assigned to either the Sham or SCI group. A moderate contusion SCI model was established as previously described [34, 44]. Briefly, a laminectomy was performed at T9-T11 under isoflurane anesthesia, and the exposed vertebral column was stabilized using a spinal cord adaptor (RWD #68094). The vertebral bone overlying the T10 spinal cord was removed, and a moderate impact (60 kilodyne) was delivered to the exposed dorsal surface using the Infinite Horizon Spinal Cord Impactor (Precision Systems and Instrumentation). Following injury, manual bladder expression was performed at least three times daily for 7-14 days, until reflexive bladder emptying was restored. Sham mice underwent a laminectomy without impact.

Behavioral Assessments

The researchers conducting the behavioral experiments were blinded to group assignments until all assessments were completed. Locomotor function was evaluated using the Basso Mouse Scale (BMS) and BMS subscore as previously described on days 1, 3 and 7 post-injury, and then weekly until day 42 [45]. For each assessment, two independent observers blinded to group assignment monitored the performance of each mouse for 4 minutes and scored locomotor ability according to the BMS. This scale ranges from 0 (complete hindlimb paralysis) to 9 (normal locomotion), based on hindlimb joint mobility, weight-supported stepping, interlimb coordination, toe clearance, trunk stability, and tail position. In addition to BMS scoring, the proportion of animals exhibiting coordinated movements and consistent plantar stepping was also recorded.

The horizontal ladder (HL) test was used to evaluate recovery of sensorimotor coordination after SCI by assessing accurate paw placement and adaptive stepping [46, 47]. Skilled walking was assessed at 6 weeks post-SCI using a previously published protocol [48]. One day before testing, all mice were trained with 5-10 trials to traverse the horizontal ladder beam toward the home cage without turning or reversing. On the test day, trials were recorded with a Canon video camera from the underside view. For each animal, at least five successful trials-defined as continuous crossings of all 20 rungs with a full view of the hind paws and without turning or back walking-were used for analysis. Positive events were defined as plantar step, toe step, and skip, whereas negative events included slip, miss, and drag. The ladder beam score (LBS%) was calculated as the number of positive events divided by the total number of events. Cumulative errors were quantified as the total number of negative events across five trials.

Tissue Preparation

All mice were sacrificed by transcardial perfusion with ice-cold 0.9% saline using a peristaltic pump. For RNA sequencing, equivalent volumes of spinal cord tissue encompassing the lesion core and surrounding area, as well as lung and spleen, were collected from both Aged WT and Hv1 KO groups at 7- and 42-days post-SCI. Samples were immediately frozen on dry ice and stored at −80 °C until further use.

For histopathological analyses, mice were perfused with ice-cold 0.9% saline followed by cold 4% paraformaldehyde (PFA). Spinal cords were harvested, post-fixed in 4% PFA overnight at 4 °C and then cryoprotected in 30% sucrose in 0.01 M PBS for 48 h at 4 °C until they sank. Spinal cord segments were coronally sectioned at 20 µm and mounted serially on slides, arranged into 10 sets of 10 slides each. One representative slide from each set was selected for histopathological staining.

Histopathology and Quantitative Image Analysis

Luxol Fast Blue (LFB, Cat# S3382, Sigma-Aldrich) staining was performed to assess myelin content and evaluate white matter sparing after SCI, as previously described [34, 48]. The slides were rinsed in distilled water for 2 min, dehydrated sequentially in 50%, 70%, 80%, and 95% ethanol for 2 min each, and then incubated overnight in LFB solution at 57 °C. The following day, slides were rinsed with 95% ethanol, followed by distilled water, and then immersed in saturated lithium carbonate solution for 1.5 min to differentiate gray and white matter. Differentiation continued in 70% ethanol for 3 min, or until a clear distinction between gray and white matter was achieved. Finally, slides were dehydrated in 80%, 95%, and 100% ethanol, cleared in xylene, and coverslipped using permanent mounting medium. LFB-stained sections were imaged at 5× magnification under a bright-field microscope. Regions of interest (ROIs) within the white matter were traced, and both LFB-positive area and total area were quantified using ImageJ (NIH, RRID:SCR_003070). The lesion epicenter was defined as the section containing the minimal spared white matter (SWM), and residual white matter in adjacent rostral and caudal sections (200 and 400 µm intervals) was also quantified.

Lesion volume was quantified on serial sections taken at 1-mm intervals spanning 5 mm rostrally and caudally from the epicenter, as previously described [34, 48]. Sections were stained with GFAP (1:1000; Cat# Z0334, Dako) overnight at 4 °C, followed by incubation with a biotinylated secondary antibody (Vector Labs, Cat# BA-1000) for 2 h at room temperature. The chromogenic reaction was developed using diaminobenzidine (DAB) reagent (DAB Peroxidase Substrate Kit with Nickel, Vector Labs, Cat# SK-4100) for 3–10 min. Images were acquired under a bright-field microscope at 4× magnification, and total lesion volume was quantified using the Cavalieri method in Stereoinvestigator Software [34, 48].

RNA Extraction and Bulk RNA Sequencing (RNAseq)

Total RNA was extracted from spinal cord, lung, and spleen tissue samples at 7 days and 6 weeks post-SCI using the miRNeasy Mini Kit (Qiagen, Cat# 74104). The samples were sent to Novogene Bioinformatics Technology Co., Ltd. (Sacramento, CA) for RNA quality assessment, mRNA library preparation (poly(A) enrichment), and sequencing as 150 bp paired end reads on the Illumina NovaSeq 6000 platform. RNA samples with RNA Integrity Number (RIN) > 7 were processed in large batches for library construction with an input of 100 ng total RNA to minimize batch effects. Mapping of 150 bp paired-end reads to the mouse reference genome (GRCm39) with GENCODE gene annotation (version M33) was performed using the STAR aligner version 2.7.5 with the default mapping parameters [49]. Gene- and isoform-level expression at the transcripts per million (TPM) level were quantified using RSEM 1.3.3 for each sample [50]. Differentially expressed genes (DEGs) were identified using the DESeq2 package version 1.42.1 [51]. An adjusted p-value of less than 0.05 was used to identify DEGs. Subsets of DEGs displayed as heatmaps were normalized across samples as z-scores and then averaged to a single value per group before plotting. Gene ontology (GO) enrichment analysis was performed using

clusterProfiler (v4.10.1) with DEGs identified by DESeq2 [52].

Quantitative real-time PCR (qPCR)

Complementary DNA (cDNA) was generated using the Verso cDNA RT Kit (Cat# AB1453B, Thermo Scientific), following the manufacturer's instructions. qPCR of target mRNAs was carried out with TaqMan gene expression assays for Nr1d1(Mm00520708_m1), Dbp (Mm00497539_m1) and GAPDH (Mm9999 9915_g1) using a QuantStudio™ 5 Real-Time PCR System (Applied Biosystems). The target gene expression levels were normalized to the expression of GAPDH, and relative gene expression change was quantified using the $2^{-\Delta\Delta Ct}$ method with the control sample as the reference [34, 48].

Sample preparation and western blot analysis

A 5-mm segment of spinal cord tissue was collected from the lesion epicenter in the SCI group and from the corresponding T10 region in the sham group for both aged WT and Hv1KO mice. Spleen and lung tissues of comparable weight were also harvested from the same animals. All tissues were rapidly frozen on dry ice and stored at −80 °C. Western blot analysis was performed as previously described [34]. In brief, tissues were homogenized in ice-cold RIPA lysis buffer (Cat# R0278, Sigma-Aldrich) with protease inhibitor cocktail (Cat# P8340, Sigma-Aldrich), phosphatase inhibitor cocktail 2 (Cat# P5726, Sigma-Aldrich), and phosphatase Inhibitor Cocktail 3 (Cat# P0044, Sigma-Aldrich), followed by sonication and centrifugation. After collecting supernatant, protein concentration of each tissue sample was measured by the Pierce BCA method (Cat# 23227, Thermo-Fisher Scientific). Equal amounts of total protein were loaded into a 4-20% SDS-Page gel (Bio-Rad, US) and then transferred to a 0.2 µm nitrocellulose membrane (Bio-Rad, US). After blocking with 5% non-fat skim milk in PBST, membranes were incubated overnight at 4 °C with the following primary antibodies: HVCN1 (1:2000, Cat# AHC-001, Alomone), NR1D1 (REV-ERBα) (1:1000, Cat# ab174309, Abcam), DBP (1:1000, Cat# 12662-1-AP, Proteintech), CIART (C1orf51) (1:1000, Cat# ab174309, Invitrogen), cGAS (1:1000; Cat# 31659, Cell Signaling Technologies), STING (1:1000, Cat# 13647, Cell Signaling Technologies), Wnt3a (1:1000, Cat# CST-2721, Cell Signaling Technologies), Iba1 (1:1000, Cat# CST-17198, Cell Signaling Technologies), Integrin α9 (1:1000, Cat# ab140599, Abcam), Tyrosine hydroxylase (TH, 1:5000, Cat# SIG-AB152, MilliporeSigma), β-actin (1:10,000; Cat# A1978, MilliporeSigma), and GAPDH (1:10000; Cat# 607905, BioLegend). Next day, the membranes were incubated with HRP-conjugated secondary antibodies for 1 hour. The immunoblots were visualized with SuperSignal West Dura Extended Duration Substrate (Cat# 34076, Thermo-Fisher Scientific) and imaged using a ChemiDoc™ MP system (Bio-Rad). The quantification of optical density of signal bands was performed using the Image Lab software (Bio-Rad) according to the manufacturer's instructions using β-actin and GAPDH as the loading control. All data are expressed as fold-change relative to the Sham/WT group.

Pharmacological inhibition of Hv1 in aged C57BL/6 mice

Aged (22-month-old) male C57BL/6 mice (Charles River) subjected to moderate SCI were treated with 2-Guanidinobenzimidazole (2-GBI; Cat# G11802, Sigma-Aldrich), which binds to the intracellular voltage-sensing domain of Hv1 and inhibits its proton conduction [53-55]. Mice were weighed and administered 2-GBI (dissolved in 10% DMSO, 10 mg/kg body mass) [56, 57] or vehicle alone by daily intraperitoneal injection for 7 days, beginning 30 minutes post-injury. BMS scores were recorded on days 1, 3, 5, and 7 after SCI. A 5-mm spinal cord segment centered on the lesion site was collected for Western blot analysis.

Statistical Analysis

Data are presented as mean ± standard error of the mean (SEM) from the indicated number of independent experiments, with individual data points shown in each graph. Statistical analyses were performed using GraphPad Prism (version 10.2.0; GraphPad Software, Inc., La Jolla, CA). Data normality was assessed using the Shapiro–Wilk test. BMS scores and subscores were analyzed by two-way analysis of variance (ANOVA) with repeated measures, followed by Sidak's multiple comparisons post hoc test. For comparisons among multiple groups, one-way or two-way ANOVA was used, followed by Tukey's multiple comparisons post hoc test for parametric data. Nonparametric data were analyzed using the Mann–Whitney test. GO analysis was performed using a one-sided Fisher's exact test with multiple-hypothesis correction *via* the Benjamini–Hochberg method. DEG analysis used the Wald test, with p-values similarly adjusted using the Benjamini–Hochberg procedure. Detailed statistical analyses for each assay are provided in the figure legends. A p-value < 0.05 was considered statistically significant.

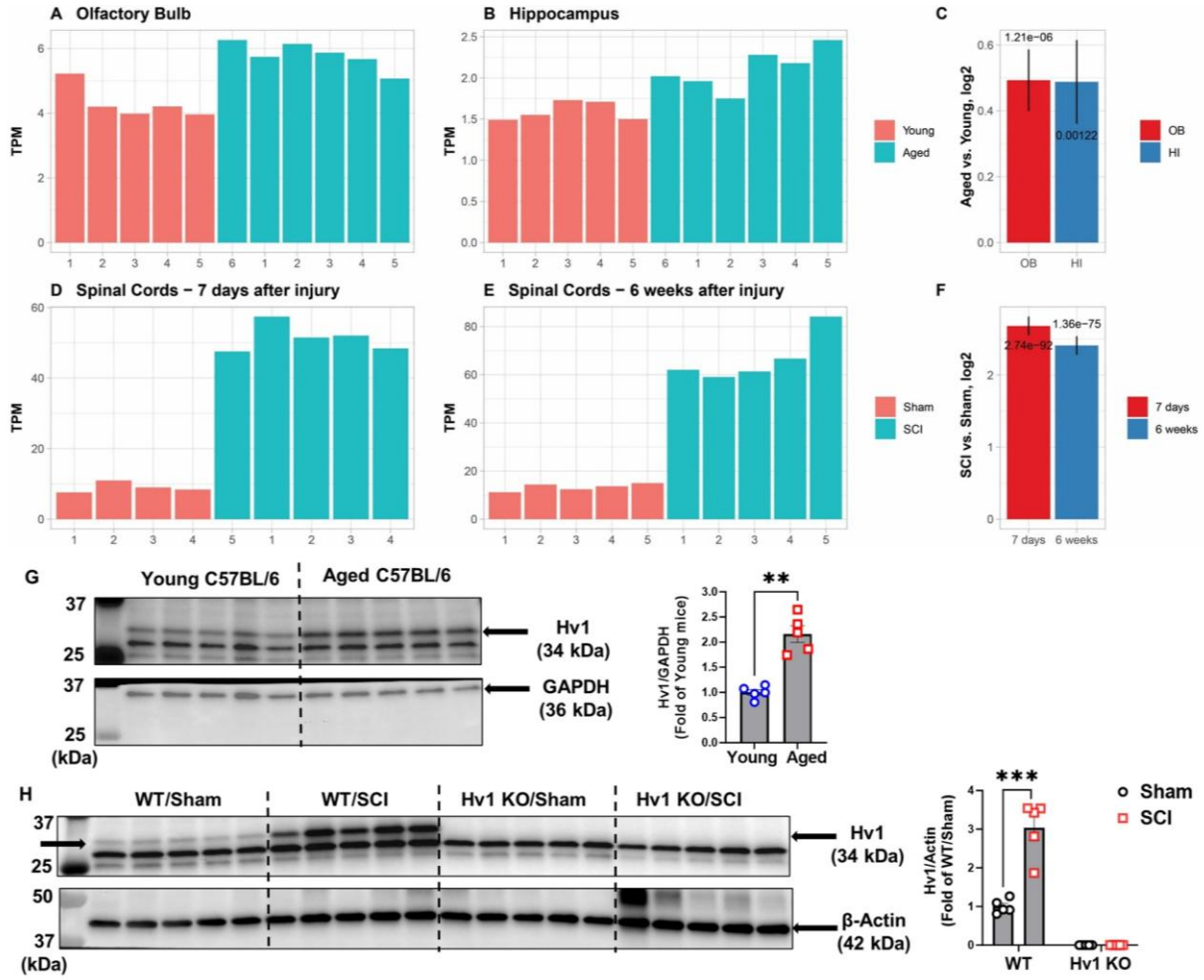

Figure 1. Old age and SCI lead to upregulation of Hv1 gene and protein expression levels. (A-C) Expression levels of *Hvcn1* in the olfactory bulb (A) and hippocampus (B) of young (3-month-old) and aged (20-month-old) C57BL/6 male mice, demonstrating significant age-related upregulation (C). **(D-F)** In aged C57BL/6 mice, SCI further increased Hvcn1 expression at both acute (7d, D) and chronic (6w, E) timepoints, with statistical significance shown in (F). Statistical analysis was performed with the Benjamini-Hochberg method and presented as adjusted p-values. n=4-5 mice/group. **(G-H)** The protein expressions of Hv1 in spinal cord tissue were analyzed by Western blot with GAPDH and β-Actin as loading control, respectively. Sham-aged mice exhibited a 2.2-fold increase relative to young mice (G, unedited western blots in Supplementary Fig. 1). At six weeks post-injury, SCI/WT mice exhibited a threefold elevation in Hv1 protein expression relative to Sham/WT controls (H, unedited western blots in Supplementary Fig. 1). Hv1 protein was undetectable in Hv1 KO mice. n=5 mice/group. *p<0.05 vs. young mice with Mann Whitney test. ***p<0.001 vs. WT/Sham mice. Two-way ANOVA following Tukey's multiple comparisons test.

RESULTS

Hvcn1 expression is upregulated with aging and following SCI

As a first step towards exploring and confirming the connection between Hv1 and age, we used RNAseq data from a prior study [58] (GEO# GSE297195) to compare the expression levels of the *Hvcn1* gene in young adult (3-month-old) and aged (20-month-old) male C57BL/6 mice. For quantification, the relative abundance of each sample was represented as Transcripts per Million (TPM) to account for both transcript length and sequencing depth. In the olfactory bulb (Fig.1A) and hippocampus (Fig.1B) regions, we observed a significant increase of up to 40% in transcript abundance, with an adjusted p-value of 1.21e-6 and 0.00122 respectively (Fig. 1C). By subjecting aged 20-month-old male C57BL/6 mice to a moderate SCI, we observed a marked upregulation of the *Hvcn1* gene by up to 6-fold in the spinal cord tissue (SPC) at 7d (Fig. 1D) and 6w (Fig. 1E) post-injury. Statistical analysis of the relative abundance by the Benjamini-Hochberg method yielded p-values at 2.74e-92 and 1.36e-75 for 7d and 6w timepoints respectively (Fig. 1F). At the protein level, Western blot analysis showed a 2.2-fold increase in SPC in sham-aged mice compared with young

mice ($p<0.01$; Fig. 1G, Supplementary Fig. 1). At 6 weeks post-injury, Hv1 protein expression was elevated three-fold in SCI/WT mice relative to Sham/WT controls ($p<0.001$; Fig. 1H, Supplementary Fig. 1). As expected, Hv1 protein was undetectable in Hv1 KO mice, confirming the efficacy of our constitutive knockout strain. Taken together, these findings indicate that Hv1 expression is higher in aged than in young mouse brains, and that SCI further elevates Hv1 levels in the injured SPC. These results highlight the critical role of Hv1 in the heightened inflammatory response to SCI in aging.

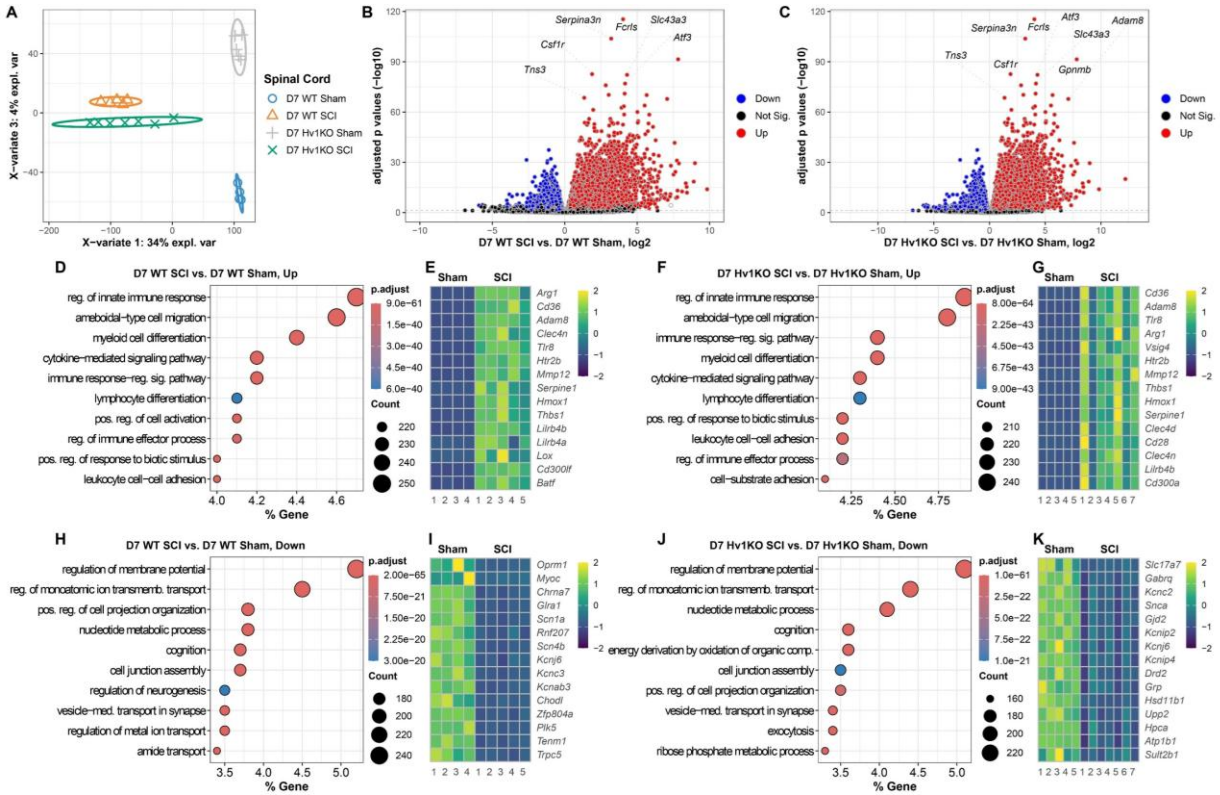

Figure 2. SCI induces distinct transcriptomic signatures in the spinal cords of aged WT and Hv1 KO mice at 7 days post-injury. (A) PLS-DA of normalized transcriptomes across all groups. **(B–C)** Volcano plots of DEGs in WT/SCI vs. WT/Sham (B) and Hv1 KO/SCI versus Hv1 KO/Sham (C). **(D–G)** GO molecular process enrichment of upregulated DEGs with corresponding heatmaps: WT/SCI vs. WT/Sham (D–E) and Hv1 KO/SCI vs. Hv1 KO/Sham (F–G). **(H–K)** GO molecular process enrichment of downregulated DEGs with corresponding heatmaps: WT/SCI vs. WT/Sham (H–I) and Hv1 KO/SCI vs. Hv1 KO/Sham (J–K). Heatmaps display relative expression levels, with warmer hues denoting increased expression and cooler hues denoting reduced expression. n=4 (WT/Sham), 5 (WT/SCI), 5 (Hv1 KO/Sham), and 7 (Hv1 KO/SCI) mice.

SCI induces distinct transcriptional changes in the spinal cord of aged WT and Hv1 KO mice

To examine acute-stage molecular changes in the SPC of aged WT and Hv1 KO mice following SCI, we performed RNAseq on tissue collected from the injury site at 7 days post-injury. PLS-DA of all normalized gene counts showed clear separation between the four groups (Fig. 2A). Baseline genotype differences between KO/Sham vs. WT/Sham revealed differences in genetic background, with genes like *Ubc*, *Hoxc11*, and *Ide* being significantly downregulated in the volcano plot (Supplementary Fig. 2A), whereas markedly upregulated genes only included *Mid1* and *Gm49980*. Consequently, pathway enrichment analysis only yielded GO terms for downregulated genes, showing genes involved in "synaptic vesicle cycle", "leukocyte homeostasis" and "regulation of generation of precursor metabolites and energy" (Supplementary Fig. 2B), which included notable genes like *Slc10a4*, *P2rx7*, and *Cd24a* (Supplementary Fig. 2C). Further examination of DEGs with a false discovery rate (FDR) of less than 0.05 showed dramatic changes in SCI vs. Sham groups for both WT (Fig. 2B) and Hv1 KO mice (Fig. 2C). Pathway enrichment analysis by GO terms showed distinct pathways being activated in the two different genotypes (Fig. 2D-K). Although the top two upregulated pathways in both WT/SCI vs. WT/Sham (Fig. 2D) and KO/SCI vs. KO/Sham (Fig. 2F) included "regulation of innate immune response" and "ameboidal-type cell migration", the third pathway in WT mice was "myeloid cell

differentiation", whereas Hv1 KO mice showed more abundance in "immune response-regulation signaling pathway". Similarly, the third top downregulated pathway were also different, with WT mice (Fig. 2E) showing more enrichment in pathways related to "positive regulation of cell projection organization", while the KO mice (Fig. 2G) showed more abundance in "nucleotide metabolic process". Moreover, specific gene ratios were also distinct between the two genotypes (Fig. 2H-K), with KO mice showing higher gene counts in pathways like "lymphocyte differentiation" and "positive regulation of response to biotic stimulus", suggesting that SCI activated different pathway in WT and KO mice, prompting a diverse immune response. For quantification, gene expression levels within each enriched pathway were illustrated as bar graphs, with TPM plotted on the y-axis (Supplementary Fig. 3). Together, these findings demonstrate that although both WT and Hv1 KO mice elicit strong immune responses during the acute stage of SCI, Hv1 ablation reshapes transcriptional programs toward distinct immune-regulatory and metabolic pathways, underscoring genotype-specific mechanisms of injury response.

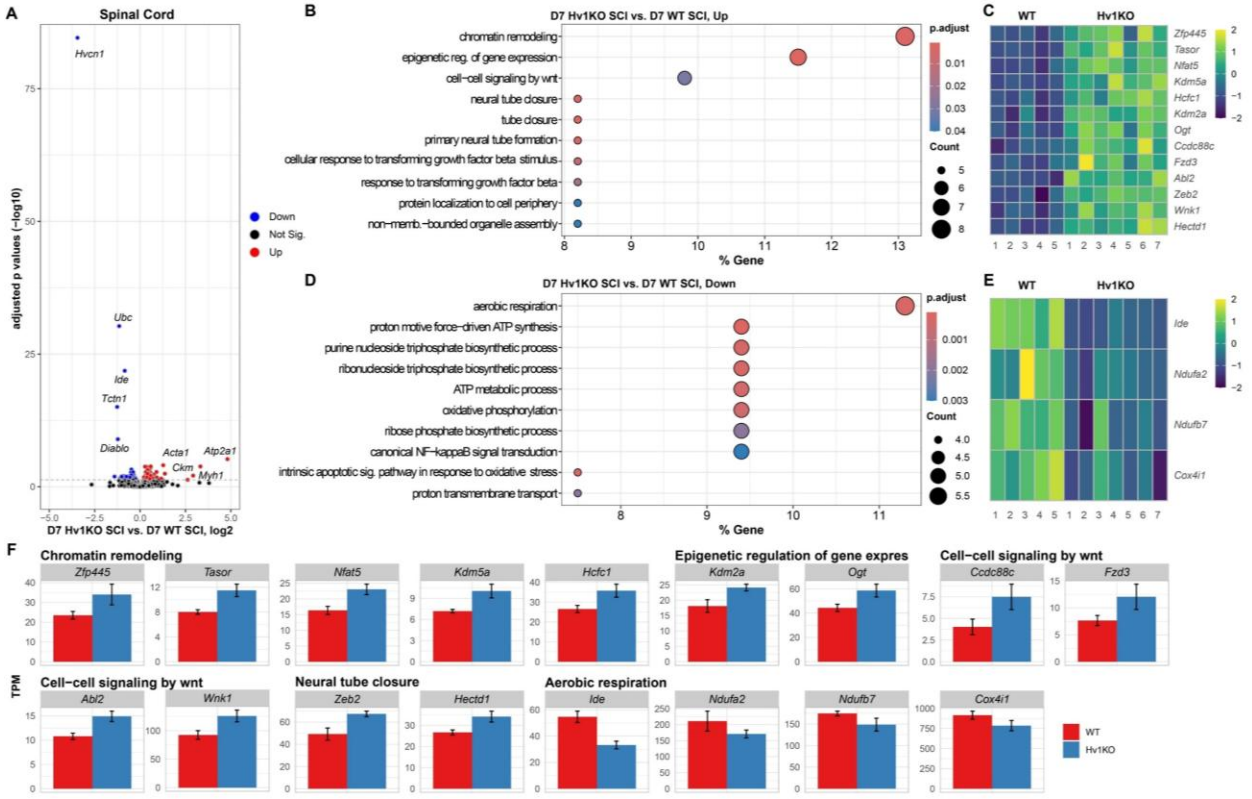

Figure 3. Hv1 ablation alters acute transcriptomic responses in the spinal cord of aged mice seven days post-injury. (A) Volcano plot of all DEGs derived from Hv1 KO/SCI vs. WT/SCI comparison. (**B-C**) Pathway enrichment analysis with Gene Ontology molecular processes of upregulated DEGs (B) and heatmap of genes associated with the top four upregulated pathways (C). **(D-E)** Pathway enrichment analysis with GO molecular processes of downregulated DEGs (D) and heatmap of genes associated with the top four downregulated pathways (E). **(F)** Bar graph of genes within the top up- and downregulated pathways. n=5 (WT/SCI) and 7 (Hv1 KO/SCI) mice.

We next examined key genotypic differences in the SPC region of WT/SCI and KO/SCI mice at 7d post-injury to identify early molecular changes driving pathological or neuroprotective cascades. DEGs analysis further identified pronounced transcriptional shifts in the KO/SCI mice relative to WT/SCI group (Fig. 3A). Although some downregulated genes (*Ubc*, *Ide*, *Diablo*) overlap with KO/Sham vs. WT/Sham, many upregulated genes (*Acta1*, *Ckm*, *Myn1*, *Atp2a1*) were unique to post-injury groups, suggesting an interaction between SCI and Hv1 ablation in aged mice. Pathway enrichment analysis showed "chromatin remodeling", "epigenetic regulation of gene expression", "cell-cell signaling by Wnt", and "neural tube closure" as the top pathways being upregulated in KO/SCI compared to WT/SCI animals (Fig. 3B-C). On the other hand, top downregulated pathways included "aerobic respiration", "proton motive force-driven ATP synthesis", and "purine nucleoside triphosphate biosynthetic" (Fig. 3D-E). Notable DEGs of the top upregulated pathways (Fig. 3C) included *Zdfp445,*

Tasor, Nfat5, Hcfc1, and genes that encode Jumonji domain proteins (*Kdm5a, Kdm2a*). In contrast, notable DEGs of the top downregulated pathway include *Ide, Ndufa2, Ndufb7 and Cox41* (Fig. 3E). Gene-level expression of key DEGs in up- and downregulated pathways was shown as bar graphs with TPM-normalized values (Fig. 3F). Together, these results suggest that aged Hv1 KO protects the injured SPC by promoting repair and stem cell differentiation while reducing oxidative stress and senescence.

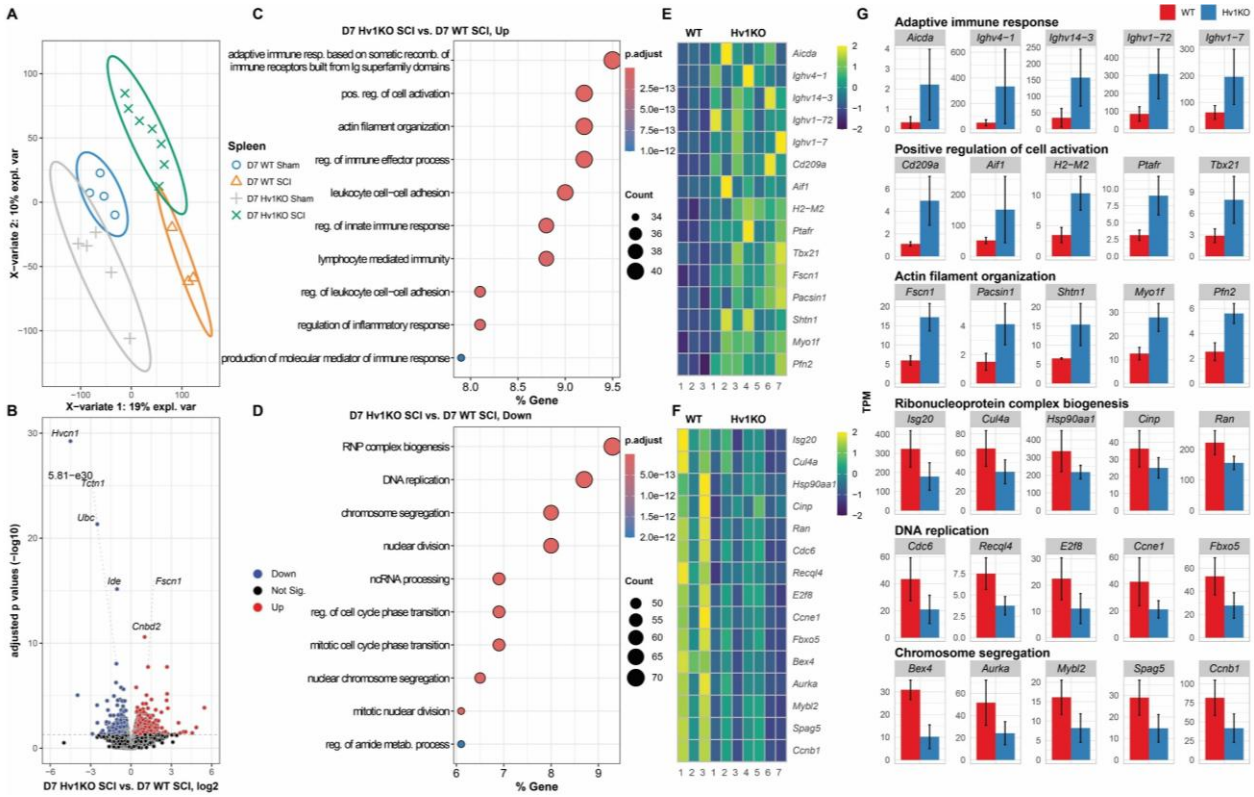

Figure 4. Hv1 deficiency enhances splenic immune activation while suppressing cell cycle programs at 7 days post-SCI in aged mice. (A) PLS-DA of normalized transcriptomes for each group**. (B)** Volcano plot displaying DEGs in Hv1 KO/SCI vs. WT/SCI. **(C-D)** Pathway enrichment analysis by GO molecular processes of up- (C) and downregulated (D) genes. **(E-G)** Heatmap of signature genes derived from the top three up- (E) and downregulated (F) pathways in GO analysis, along with bar graphs of normalized TPM for quantification (G). n=4 (WT/Sham), 3 (WT/SCI), 5 (Hv1 KO/Sham), and 7 (Hv1 KO/SCI) mice.

RNA sequencing reveals systemic spleen and lung changes after SCI and Hv1 deletion

Having established the transcriptional landscape at the injury site, it is important to recognize that SCI triggers a systemic response extending beyond the CNS [59, 60]. We next examined systemic responses to SCI. The spleen, a reservoir for immune cells [20], and the lung, prone to secondary inflammation [21], were analyzed by RNAseq at 7 days post-injury. Both tissues showed distinct immune signatures, highlighting the systemic impact of SCI and effects of Hv1 ablation.

In the spleen, we observed a clear separation between the four groups after PLS-DA of all normalized gene counts (Fig. 4A), while the volcano plot revealed robust changes in specific genes when comparing between KO/SCI and WT/SCI (Fig. 4B). Results from GO enrichment analysis revealed "adaptive immune response based on somatic recombination of immune receptors built from immunoglobulin superfamily domain", "positive regulation of cell activation", and "actin filament organization" as the top pathways being upregulated in the Hv1 KO (Fig. 4C), while the terms "ribonucleoprotein complex biogenesis", "DNA replication" and "chromosome segregation" were the most downregulated pathways (Fig. 4D). Notable DEGs for this comparison included *Aicda* (Activation Induced Cytidine Deaminase), *Il10* (Interleukin 10), *Cd209a* (cluster of differentiation 209 antigen) amongst the significantly upregulated genes (Fig. 4E), along with several genes from the immunoglobulin heavy chain variable region (*Ighv4-1, Ighv14-3, Ighv1-72, Ighv1-7*). Alternatively, the top downregulated DEGs included *Isg20* (Interferon Stimulated Exonuclease Gene 20) (Fig.

4F), which has been reported to have high expression levels in lymphoid tissues and immune cell subtypes (B-cells, plasma cells, dendritic cells, neutrophils), which are crucial for antiviral defense and chronic inflammation seen with aging [61].

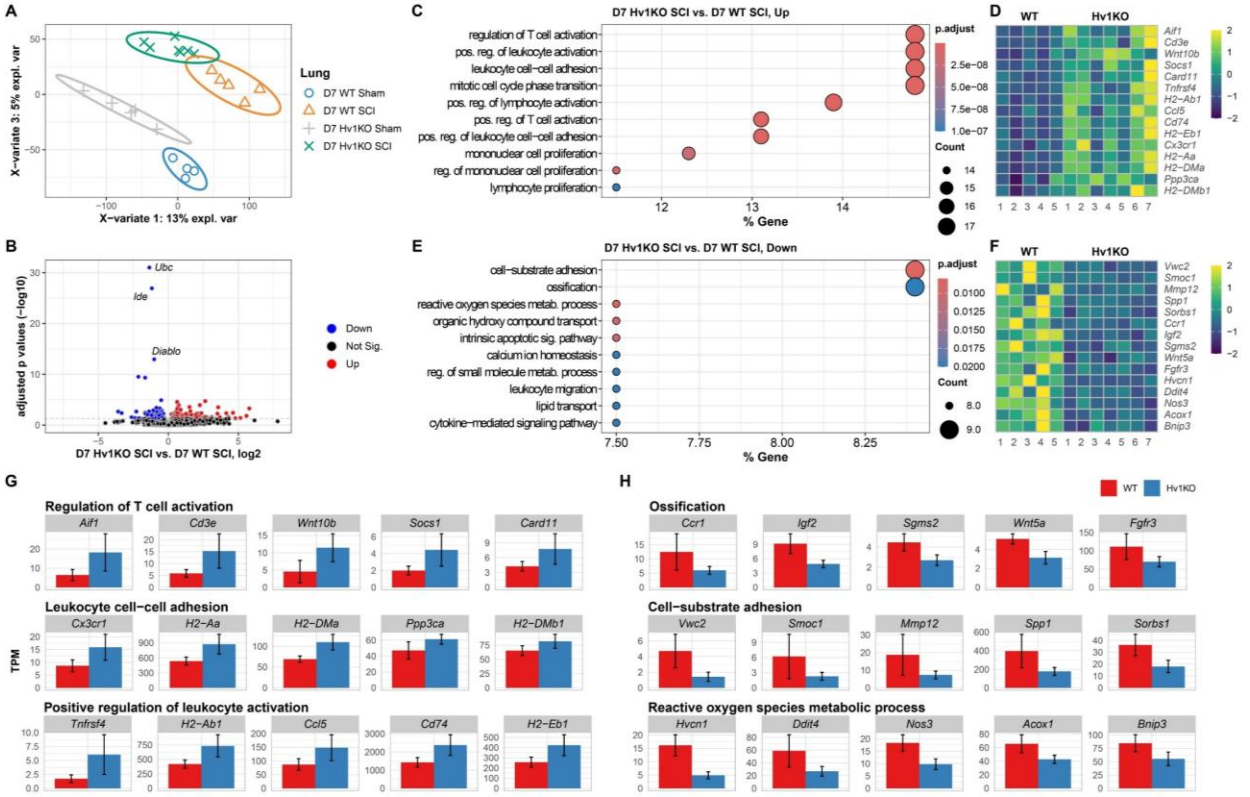

Figure 5. Lung transcriptomic profiling at 7d post-SCI reveals altered immune and metabolic pathways in Hv1 aged KO mice. **(A)** PLS-DA showing clear separation of lung transcriptomes across groups. **(B)** Volcano plot of differentially expressed genes (DEGs) comparing Hv1KO/SCI vs. WT/SCI. **(C-F)** Enriched GO molecular processes for upregulated (C) and downregulated (E) DEGs. Heatmaps of representative genes contributing to the top enriched pathways (D, F). **(G–H)** Bar plots illustrating expression of selected DEGs linked to immune regulation (G) and metabolic/structural pathways (H). n=4 (WT/Sham), 5 (WT/SCI), 5 (Hv1 KO/Sham), and 7 (Hv1 KO/SCI) mice.

Although this study only observed age-dependent upregulation of *Isg20* in circulating immune cells, these cellular changes reflect similar aging-associated alterations in spleen-resident immune cells, as the spleen serves as a major reservoir for NK cells, dendritic cells, and other lymphocytes. The upregulation of *Isg20* is likely a component of broader immunosenescence processes impacting the spleen's function in aging. Another DEG of interest is *Cul4a* (Cullin 4A), a highly expressed molecule in the spleen that's part of an E3 ubiquitin ligase complex, which targets key cell cycle and DNA repair regulators for degradation. Quantitative representation of gene expression within enriched pathways is shown as bar graphs, with TPM values on the y-axis providing normalization for library size and sequencing depth (Fig. 4G). Furthermore, transcriptomic profiles of the WT/SCI vs. WT/Sham and KO/SCI vs. KO/Sham comparisons at 7d post-injury showed distinct expression profile patterns in the volcano plots, along with differentially activated pathways in the GO analysis (Supplementary Fig. 4). Upregulated pathways in WT mice showed increased levels of genes pertaining to "chromosome segregation", "mitotic cell cycle phase transition", and "nuclear division". In contrast, the top upregulated DEGs in KO mice were mainly involved in pathways that mediate functions like "response to peptide", "proteasome-mediated ubiquitin-dependent protein catabolic process", and "chromatin remodeling". For the top enriched pathways in downregulated DEGs, WT mice had "leukocyte cell-cell adhesion" as the pathway with the lowest adjusted p-value and highest gene ratio, while KO mice showed "ameboidal-type cell migration" as the top pathway. Further examination on the baseline transcriptional differences in aged Hv1 KO and WT mice showed stark differences in genes profile (Supplementary Fig. 5A), with Hv1 KO mice showing higher expression of genes related to "production of molecular mediator of immune response" (Supplementary Fig. 5B-C), while genes that regulate "adaptive immune response lymphocyte mediated immune" were part of the top

downregulated pathways (Supplementary Fig. 5D-E). Together, transcriptional profiling revealed distinct immune responses in aged Hv1 KO spleens compared to WT, indicating a shift in peripheral immune cells that may contribute to injury-site pathology.

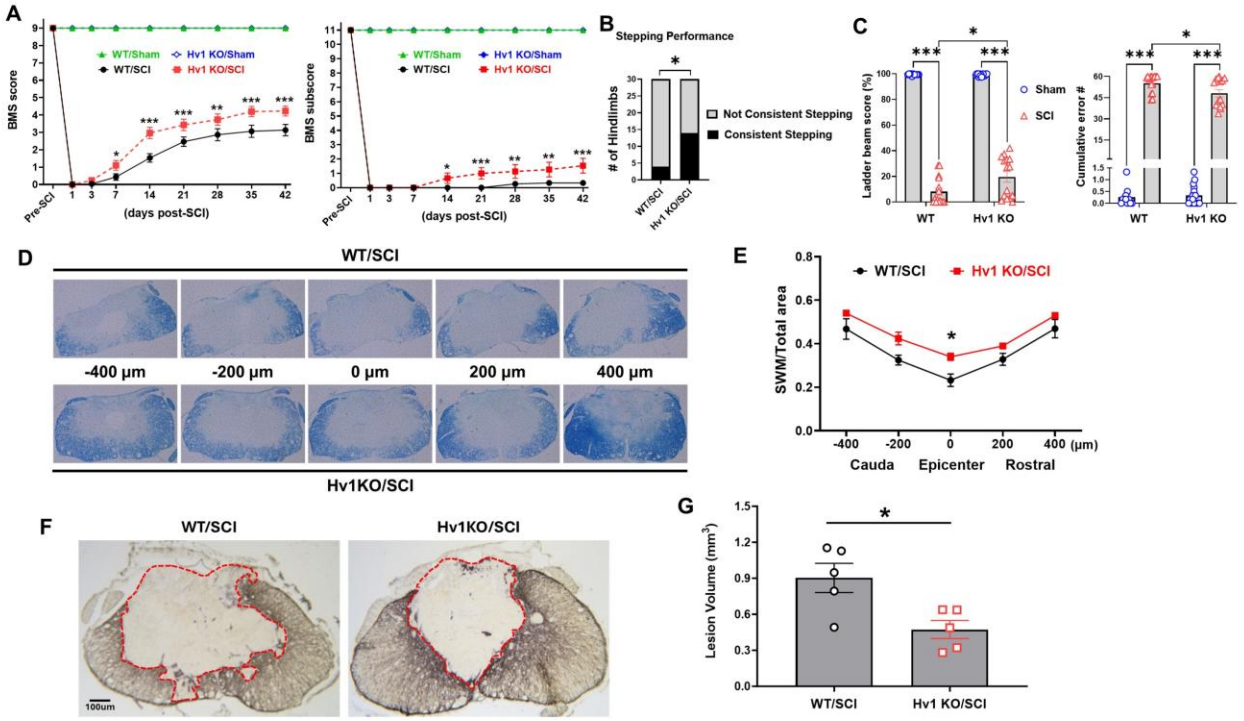

Figure 6. Hv1 depletion enhances long-term locomotor functional recovery and reduces tissue damage in aged mice following SCI. (A) Hindlimb locomotor function was assessed on days 1, 3, and 7 post-SCI, and then weekly, in aged Hv1 KO and WT mice along with their respective sham controls. Aged Hv1KO mice showed significantly higher BMS scores and subscores compared to WT mice. Two-way ANOVA with repeated measurement following Holm-Sidak's multiple comparisons test. **(B)** Hv1 deletion markedly enhanced stepping performance at 42 days post-injury compared with WT mice. Fisher's exact test. **(C)** The horizontal ladder test was conducted at 42 days post-injury to evaluate skilled walking. Aged Hv1 KO mice demonstrated significantly higher ladder beam scores and fewer cumulative errors compared to the WT group. Two-way ANOVA with Tukey's post hoc test. **(D-E)** Representative images and quantification of spared white matter (SWM) at 6 w post-injury. Mann-Whitney test. **(F-G)** Representative images of GFAP-DAB staining and quantification of the lesion volume at 6w SCI. Unpaired t-test. For behavior tests, n=11 (WT/Sham), 16 (Hv1KO/Sham), 15 (WT/ SCI), and 15 (Hv1KO/SCI) mice. For histological studies, n=5 mice/group. *p<0.05, **p<0.01, ***p<0.001 vs. WT/SCI. Scale bar=100 μm.

Lung complications are a major cause of morbidity and mortality after SCI [22]. A 2023 study showed that 12-month-old SCI rats developed pulmonary edema and airway inflammation [62], while aging itself promotes lung cellular senescence and alters damage-associated molecular patterns [63]. To assess the impact of Hv1 ablation on aged mouse lungs after SCI, we analyzed transcription profiles at 7d post-injury, which showed clear separation by injury and genotype (Fig. 5A). Beyond baseline differences (Supplementary Fig. 6), post-injury DEGs in WT (WT/SCI vs. WT/Sham, Supplementary Fig. 6A-E) and Hv1 KO (KO/SCI vs. KO/Sham, Supplementary Fig. 6F-J) mice revealed distinct, genotype-dependent pathways. Whereas WT mice showed upregulation of genes related to "chemotaxis", "taxis" and "leukocyte migration" (Supplementary Fig. 6B-C), Hv1 KO mice had increased expression of genes involved in "wound healing", "regulation of neurogenesis" and "positive regulation of cell projection organization" (Supplementary Fig. 6G-H), indicating that KO mice may be more proactive in tissue repair during the acute stages of SCI. To delve deeper into the molecular differences of WT and Hv1 KO mice after injury, direct comparison of KO/SCI to WT/SCI mice was performed, yielding a unique set of DEGs on the volcano plot (Fig. 5B). Pathway enrichment analysis via GO term biological process showed upregulated pathways in "regulation of T cell activation", "positive regulation of leukocyte activation", "leukocyte cell-cell adhesion" (Fig. 5C), which included DEGs like *Il4i1, Aif1, Cd3e*, and *Wnt10b* (Fig. 5D). In the downregulated pathways, genes involved in processes like "cell-substrate adhesion", "ossification" and "reactive oxygen species" were amongst top enrichment GO terms (Fig. 5E), which

included DEGs like *Vwc2, Smoc1, Ccr1* and *Nos3* (Fig. 5F). Bar graphs for all up and downregulated DEGs were quantified as TPM level for direct presentation of transcriptomic expression (Fig. 5G-H). In summary, Hv1 ablation in aged mice after SCI triggers systemic spleen and lung changes with heightened immune activation, potentially enhancing resistance to later infections.

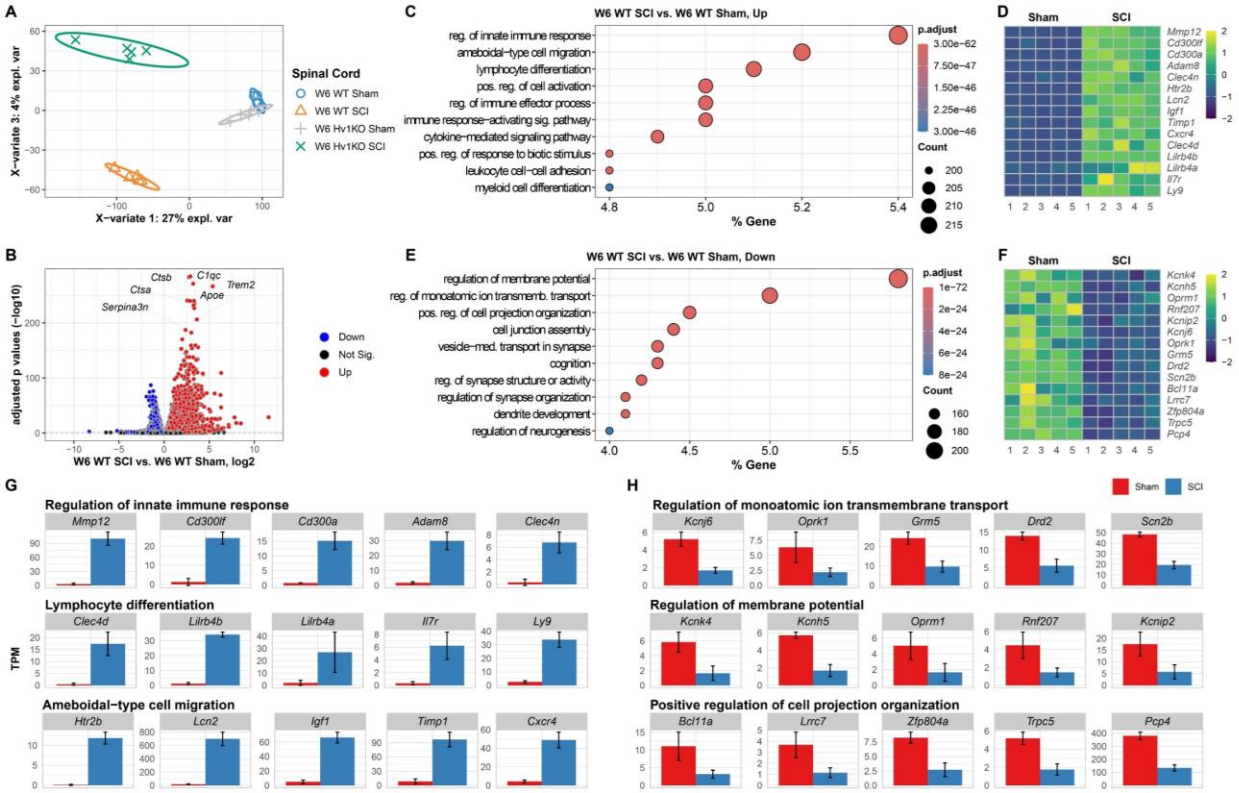

Figure 7. Chronic spinal cord transcriptomes at 6 weeks post-SCI reveal persistent immune activation and sustained suppression of neuronal programs in aged mice. (A) Multivariate analysis (PLS-DA) reveals persistent divergence of spinal cord transcriptomes by injury and genotype. **(B)** Volcano plot of differentially expressed genes (DEGs) comparing WT/SCI vs. WT/Sham. **(C–H)** GO molecular process enrichment of upregulated (C) and downregulated (E) DEGs, with representative genes displayed in heatmaps (D, F) and validated by bar plots (G, H) of immune-related and neuronal pathways. n=5 mice/group.

Hv1 depletion enhances locomotor recovery and reduces tissue damage in aged mice after SCI

Our previous study demonstrated that global Hv1 deletion in young mice significantly enhanced locomotor recovery and attenuated tissue damage after SCI [34]. To test whether SCI-induced Hv1 changes in aged mice affect inflammation or locomotor function, aged Hv1 KO mice and their WT littermates were subjected to moderate SCI. BMS analysis revealed improved locomotion in aged Hv1 KO mice compared to aged WT controls (Fig. 6A). Half of the Hv1 KO mice achieved functional recovery (BMS >3; occasional/frequent plantar stepping with partial coordination), significantly higher than WT ($p<0.05$, repeated-measures two-way ANOVA), with differences persisting to 42 days post-injury. Significant effects were observed for Post-injury Days ($F(7, 371) = 146.5$, $p<0.001$), Treatment ($F(3,53)=672.0$, $p<0.001$), and their interaction ($F(21, 371) = 52.29$, $p<0.001$). BMS subscores further confirmed improved recovery in Hv1 KO mice, significant from day 14 ($p<0.05$) through day 42 (Fig. 6B). Effects of Post-injury Days ($F(7, 371) = 6.848$, $p<0.001$), Treatment ($F(3, 53) = 1845$, $p<0.001$), and their interaction ($F(21, 371) = 4.455$, $p<0.001$) were all significant. Notably, aged Hv1 KO mice exhibited enhanced and consistent stepping performance (Fig. 6B). In the assessment of motor coordination and skilled walking, ladder beam score and the number of stepping errors showed significantly enhanced performances in aged Hv1 KO mice compared to aged WT mice (Fig. 6C). For ladder beam score, the factors of Injury ($F(1, 53) = 1042$, $p<0.001$), the factors of Genotype ($F(1, 53) = 4.405$, $P=0.04$) and the interaction of Genotype × Injury ($F(1, 53) = 4.885$, $P=0.03$) were found to be significant. For cumulative errors, the factors of Genotype ($F(1, 53) = 4.771$, $P=0.03$), Injury ($F(1, 53) = 1017$, $p<0.001$), and the interaction of Genotype × Injury ($F(1, 53) = 4.977$, $P=0.03$) were found to be significant.

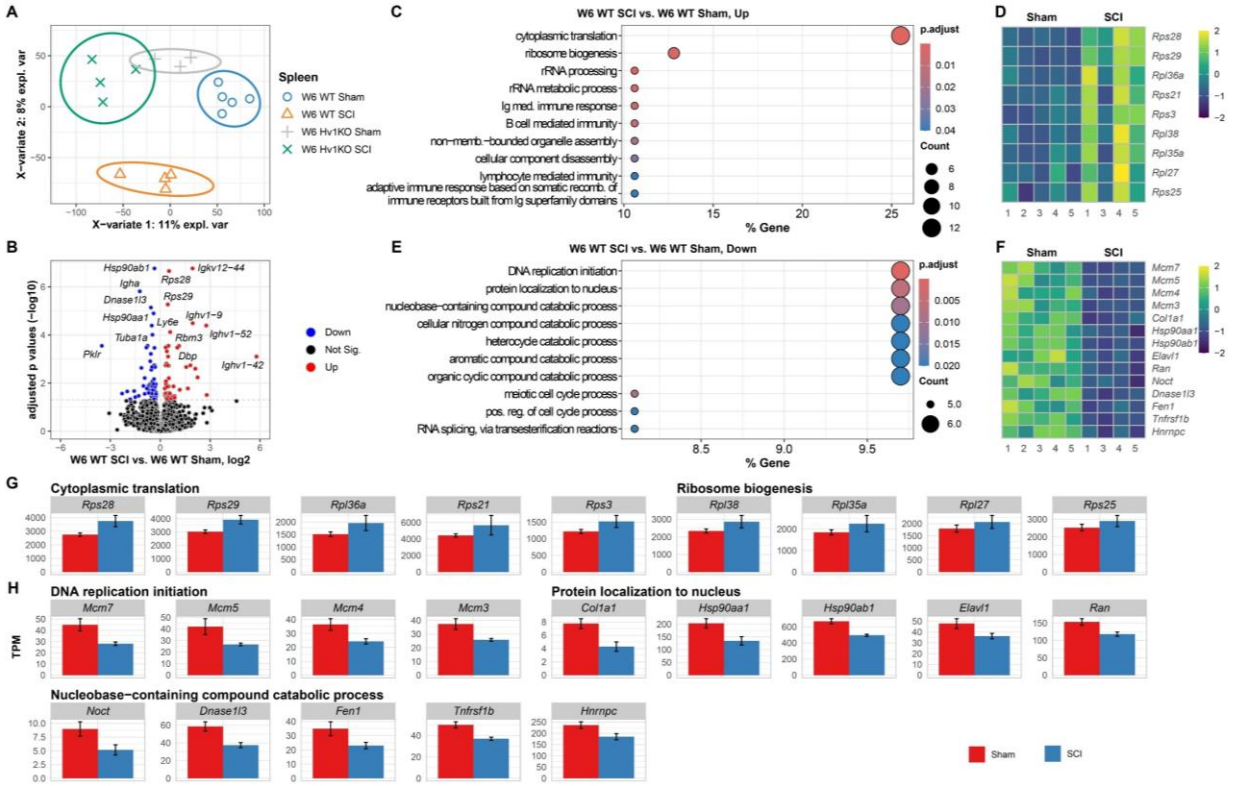

Figure 8. Chronic splenic transcriptomes at 6 weeks post-SCI show altered translational, ribosomal, and nuclear processes in aged mice. (A) PLS-DA underscores lasting transcriptomic divergence in the spleen driven by both SCI and Hv1 deficiency. **(B)** Volcano plot illustrating transcriptomic alterations in WT/SCI relative to WT/Sham. **(C–F)** GO molecular process enrichment of upregulated (C) and downregulated (E) DEGs with representative genes visualized in heatmaps (D, F). **(G–H)** Bar plots of selected DEGs grouped by functional categories, including cytoplasmic translation and ribosome biogenesis (G), and DNA replication, nucleobase catabolism, and nuclear localization (H). n=5 mice/group.

We investigated whether improved locomotor function in aged Hv1 KO mice was associated with reduced secondary tissue damage after SCI. LFB staining showed increased myelin sparing in aged Hv1 KO mice compared with aged WT mice at 42 days post-injury ($p<0.05$, Fig. 6D). Quantitative analysis revealed attenuated myelin loss at the epicenter in Hv1 KO mice ($34.0\% \pm 1.7\%$) versus WT ($23.2\% \pm 2.85\%$), with similar protection extending up to 400 µm rostral and caudal (Fig. 6E). GFAP/DAB staining further showed a 47.5% reduction in glial scar volume in Hv1 KO mice ($p<0.05$, Fig. 6G–H). These results indicate that Hv1 contributes to secondary tissue damage after SCI, and its depletion mitigates injury. Together with behavioral improvements, our findings suggest that Hv1 plays a key role in secondary damage in aged mice, where its absence enhances locomotor recovery and tissue preservation.

SCI induces chronic transcriptomic alterations in the spinal cord and peripheral organs of aged WT mice

Since SCI in aged mice causes lasting functional and structural deficits, we next probed molecular changes in the injured SPC. To capture these long-term changes, we performed RNAseq on SPC tissue at 6w post-injury, after behavioral testing. PLS-DA of the normalized transcription count showed separation of the WT/SCI and WT/Sham groups (Fig. 7A). Analysis of DEGs revealed more upregulated genes (Fig. 7B), enriched in immune-related pathways such as "regulation of innate immune response," "lymphocyte differentiation," and "cell activation" (Fig. 7C), indicating chronic neuro-inflammation in aged SPC. Amongst the downregulated DEGs, pathways that regulated membrane potential, monoatomic ion, cell projection organization and cell junction assembly are the top enriched GO process terms (Fig. 7D). Notable upregulated genes (Fig. 7E) included *Mmp12*, which promotes ECM damage, cytokine release, and demyelination [64, 65]; *Cd300lf* and *Cd300a*, regulators of macrophage-mediated efferocytosis, with *Cd300a* linked to poor recovery after SCI [66-68]; *Adam8*, a driver of cell migration and inflammation [69]; and *Lcn2*, which enhances astrocyte–microglia activation after SCI [70, 71]. In contrast, downregulated DEGs (Fig. 7F) were enriched in pathways regulating membrane potential, ion transport, cell projection organization, and

junction assembly. Key genes included potassium channel components (*Kcnk4*, *Kcnh5*, *Kcnip2*, *Kcnj6*), opioid receptors (*Oprm1*, *Oprk1*), and *Rnf207*, a co-chaperone for *HSP70*-mediated protein folding. Loss of *HSP70* has been shown to worsen lesion size and delay motor recovery [72, 73]. To facilitate rigorous quantification, expression profiles of pathway-enriched genes were depicted as bar charts, with TPM-normalized transcript levels plotted on the y-axis (Fig. 7G-H). Together, these data indicate that aged spinal cords exhibit persistent activation of immune pathways and suppression of neuronal signaling and structural genes after SCI.

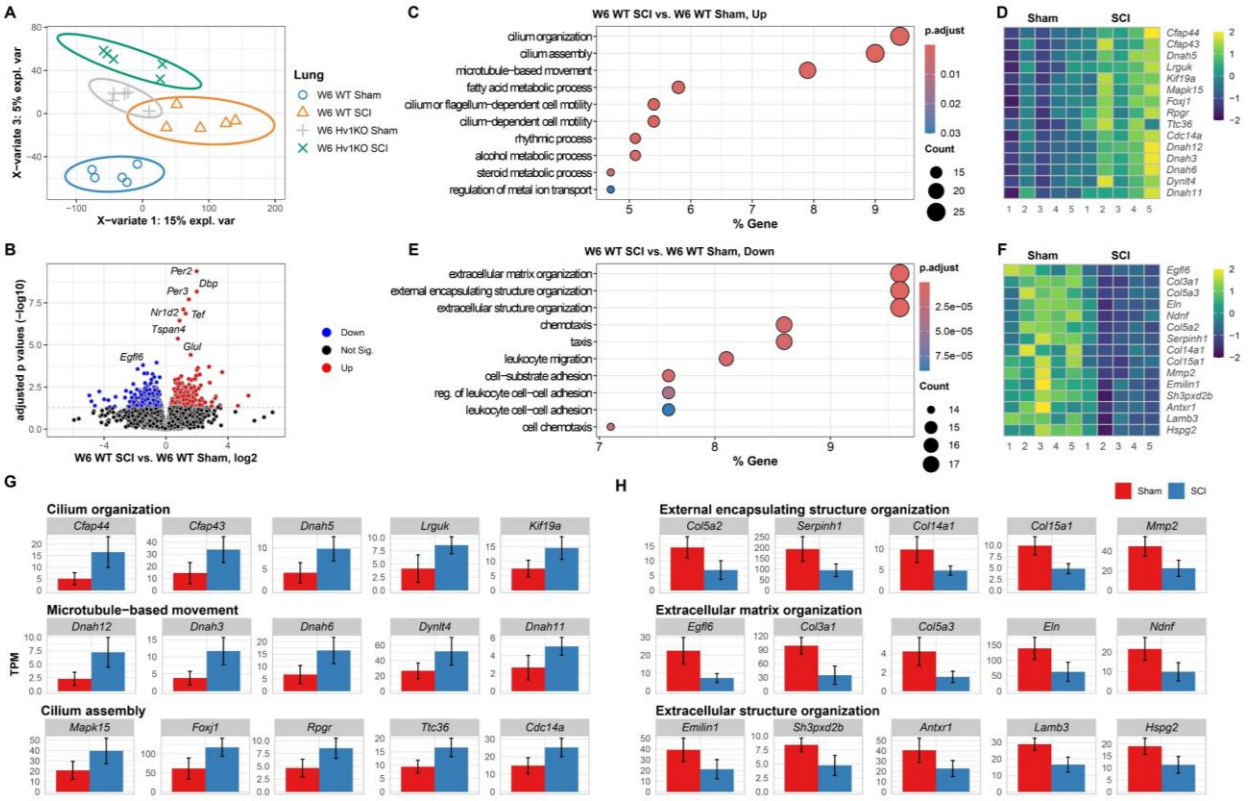

Figure 9. Chronic lung transcriptomes at 6 weeks post-SCI reveal impaired ciliary function and extracellular matrix remodeling in aged mice. (A) Global variance captured by PLS-DA highlights distinct clustering by groups according to injury and genotype. **(B)** Differential expression analysis (volcano plot) illustrating transcriptomic changes between WT/SCI and WT/Sham. **(C–F)** Functional enrichment of upregulated (C) and downregulated (E) genes with representative genes visualized in heatmaps (D, F). **(G–H)** Expression levels of selected DEGs displayed as bar plots, grouped by functional categories, including cilium organization, microtubule-based movement, and extracellular matrix/structure organization. n=5 mice/group.

In the spleen, PLS-DA demonstrated clear group separation (Fig. 8A), indicating that injury status and Hv1 ablation drive distinct transcriptional signatures. SCI in aged WT mice caused marked transcriptomic changes (Fig. 8B), with upregulation of pathways in cytoplasmic translation, ribosome biogenesis, and rRNA processing (Fig. 8C). The upregulated DEGs encoded ribosomal proteins (Fig. 8D), including components of the 40S (*Rps28*, *Rps29*, *Rps21*, *Rps3*, *Rps25*) and 60S (*Rpl36a*, *Rpl38*, *Rpl35a*, *Rpl27*) subunits, suggesting enhanced protein synthesis machinery in immune organs like the spleen [74, 75]. In contrast, downregulated DEGs (Fig. 8E–F) included DNA replication genes such as MCM complex members (*Mcm7*, *Mcm5*, *Mcm4*, *Mcm3*), as well as *Col1a1*, *Hsp90aa1*, *Hsp90ab1*, and *Elavl1*. Following injury, studies show that components of the MCM are upregulated to initiate DNA replication and repair [76]. Notably, Elavl1 is normally upregulated in germinal center B cells after activation, underscoring impaired B cell–related immune responses [77]. Quantitative analyses confirmed these expression shifts (Fig. 8G–H). Together, these results show that 6 weeks post-SCI, aged mice display persistent splenic transcriptomic remodeling marked by increased ribosomal gene expression but reduced DNA replication, stress response, and B cell–associated pathways, consistent with systemic immune dysregulation.

Given these sustained splenic alterations, we next asked whether the lung, another organ vulnerable to post-SCI complications, also showed long-term transcriptomic changes. PLS-DA analysis of the four groups examined showed clear separation by injury and genotype (Fig. 9A).

Beyond the overall upregulation of DEGs evident in the volcano plot (Fig. 9B), pathway analysis revealed strong enrichment of processes related to cilium organization and assembly, cilium-dependent motility, microtubule-based movement, and fatty acid metabolism among the upregulated genes (Fig. 9C). As cilia is critical for airway clearance and epithelial homeostasis, enrichment of these pathways suggests potential long-term disruption of lung function after SCI. Upregulated DEGs (Fig. 9D) included cilia- and microtubule-related genes such as *Cfap44*, *Cfap43*, *Lrguk*, *Kif19a*, *Mapk15*, and multiple axonemal dynein heavy chain genes (*Dnah5*, *Dnah12*, *Dnah3*, *Dnah6*, *Dnah4*, *Dnah11*), consistent with increased ciliated cells or ciliary remodeling after injury [78, 79]. In the downregulated genes, GO terms included processes for extracellular matrix and structure organization, external encapsulating structure organization and chemotaxis (Fig. 9E). Downregulated DEGs (Fig. 9F) were enriched for extracellular matrix (ECM) processes and included *Egfl6*, *Eln*, *Ndnf*, *Serpinh1*, *Antxr1*, and several collagen alpha-chain genes (*Col3a1*, *Col5a3*, *Col5a2*, *Col14a1*, *Col15a1*). Given collagens' role in ECM integrity and lung elasticity [80, 81], their suppression suggests impaired alveolar maintenance and repair post-SCI. Pathway quantification (Fig. 9G-H) revealed distinct expression profiles, with marked upregulation of cilia-associated genes and downregulation of ECM components, indicating enhanced ciliary remodeling but reduced structural integrity at 6 weeks post-SCI.

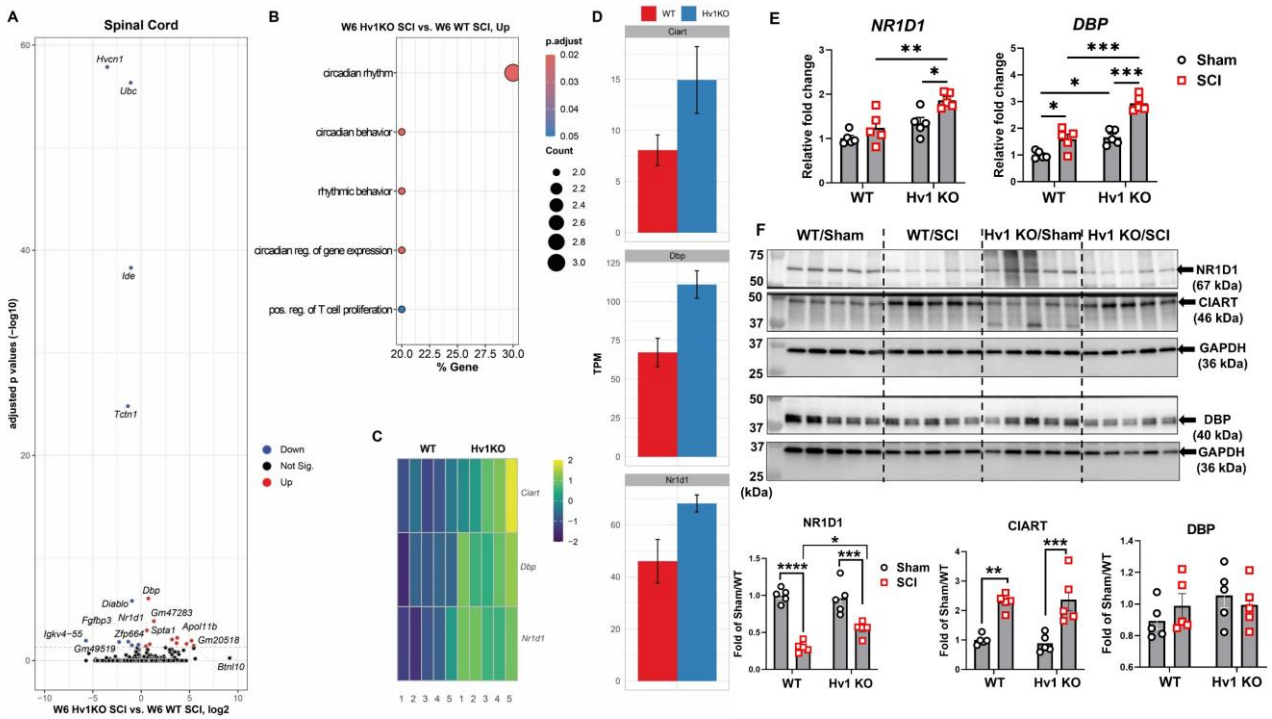

Figure 10. Hv1 deficiency alters chronic transcriptional profiles in the spinal cord of aged mice 6 weeks post-SCI. (A) Volcano plot of significantly up- and downregulated genes between Hv1 KO/SCI and WT/SCI. **(B)** GO molecular process enrichment of upregulated genes. **(C)** Heatmap of representative genes from enriched pathways. **(D)** Quantification of signature genes from top enriched processes, shown as normalized TPM in bar plots. n=5 mice/group. **(E)** qPCR analysis was performed to examine the mRNA expression level of circadian rhythm genes *NR1D1* and *DBP* in injured spinal cord tissue at 6 weeks post-SCI in both WT and Hv1KO mice. **(F)** Western blot analysis was performed to assess the protein expression levels of NR1D1, CIART, and DBP over the six-week period following SCI, and representative blots are shown (unedited western blots in Fig. S9). Protein levels were quantified by densitometry, normalized to GAPDH, and presented as fold changes relative to the WT/Sham group. n=5 mice/group. *p<0.05, **p<0.01, and ***p<0.001 Two-way ANOVA following Tukey's multiple comparisons test.

Aged Hv1 KO mice display improved transcriptomic profiles in the spinal cord and peripheral tissues following SCI

To investigate the molecular basis of Hv1 deletion-mediated benefits after SCI, we performed RNA-seq at the injury site 6 weeks post-injury. Baseline transcriptomic comparison between aged KO/Sham and WT/Sham mice identified numerous DEGs (Supplementary Fig. 7A). Enriched pathways showed upregulation of innate immune response, lymphocyte differentiation, and cell activation (Supplementary Fig. 7B), with notable genes including *Lbp*, *Cd36*, *Serping1*, *Igf2*, *Il7r*, *Ccl21a*, and *Ccl2* (Supplementary Fig. 7C).

Downregulated pathways were enriched for GO terms related to membrane potential regulation, ion transport, synaptic vesicle transport, and exocytosis (Supplementary Fig. 7D), with representative genes such as *Slc7a7*, *Tac1*, *Cck*, *Glra3*, and *Snap25* (Supplementary Fig. 7E). Analysis of SCI in Hv1 KO mice revealed numerous upregulated DEGs in KO/SCI vs. KO/Sham (Supplementary Fig. 8A), enriched for "regulation of innate immune response," "lymphocyte differentiation," and "positive regulation of cell activation" (Supplementary Fig. 8B-C). Downregulated genes were mainly associated with membrane potential regulation, monoatomic transmembrane transport, and synaptic vesicle-mediated transport (Supplementary Fig. 8D-E).

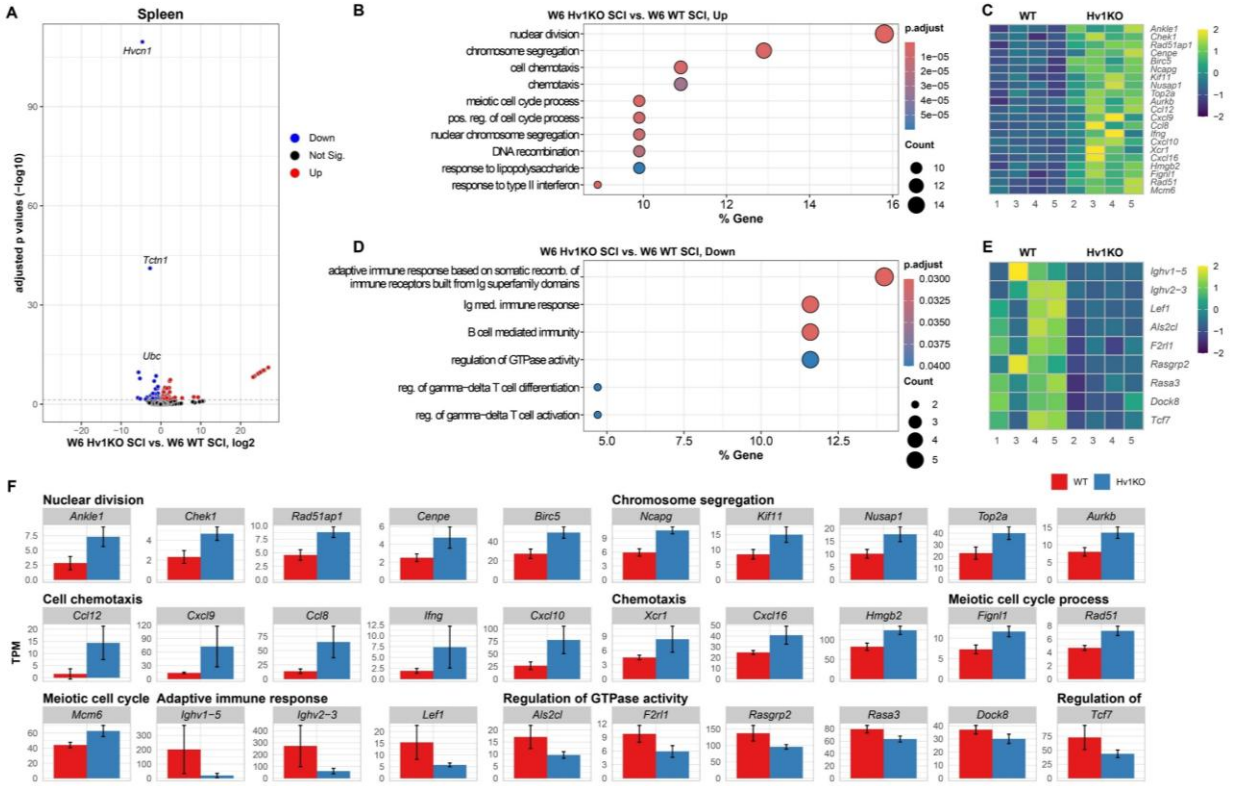

Figure 11. Ablation of Hv1 alters chronic transcriptional profiles in the spleen 6 weeks post-SCI. (A) Volcano plot illustrating transcriptomic alterations in Hv1 KO/SCI relative to WT/SCI. **(B–E)** GO molecular process enrichment of upregulated (B) and downregulated (D) DEGs with representative genes visualized in heatmaps (C, E). **(F)** Bar plots of normalized TPM values for signature genes, grouped by their top enriched biological processes. n=5 mice/group.

To be noticed, comparing KO/SCI to WT/SCI revealed few DEGs with FDR < 0.05 (Fig. 10A), resulting in only upregulated DEGs appearing in GO analysis (Fig. 10B), including circadian rhythm, rhythmic behavior, circadian gene regulation, and positive T cell proliferation. Key genes in these pathways (*Ciart*, *Dbp*, and *Nr1d1*) are shown as bar graphs for quantification (Fig. 10C-D). To investigate whether Hv1 deletion-mediated functional improvements after SCI was driven by the regulation of circadian rhythms, we examined the expression change of circadian rhythm genes and proteins. qPCR analysis showed that the circadian rhythm gene *NR1D1* was significantly upregulated in Hv1 KO mice compared to WT mice at 6 weeks post-SCI (Fig. 10E). In Hv1 KO mice, *NR1D1* mRNA expression was also higher after SCI than in Sham controls (Fig. 10E). Similarly, the expression of another circadian rhythm gene, *DBP*, was markedly increased in Hv1 KO/SCI mice compared with WT/SCI mice (Fig. 10E). Moreover, DBP expression was significantly elevated after SCI relative to Sham in both WT (p=0.0306) and Hv1 KO mice (p<0.001) (Fig. 10E). At the protein level, NR1D1 expression was significantly higher in Hv1 KO/SCI mice than in WT/SCI mice (p=0.042, Fig. 10F, Supplementary Fig. 9). Relative to Sham, SCI caused a marked reduction in NR1D1 protein expression in both WT (p<0.001) and Hv1 KO mice (p<0.001) (Fig. 10F, Supplementary Fig. 9). In contrast, the protein expression of the circadian gene CIART was substantially increased after SCI compared with Sham in both WT (p=0.003) and Hv1 KO mice (p<0.001) (Fig. 10F, Supplementary Fig. 9). However, no significant differences in DBP protein expression were detected between SCI and Sham groups or between WT and Hv1 KO mice (Fig. 10F, Supplementary Fig. 9).

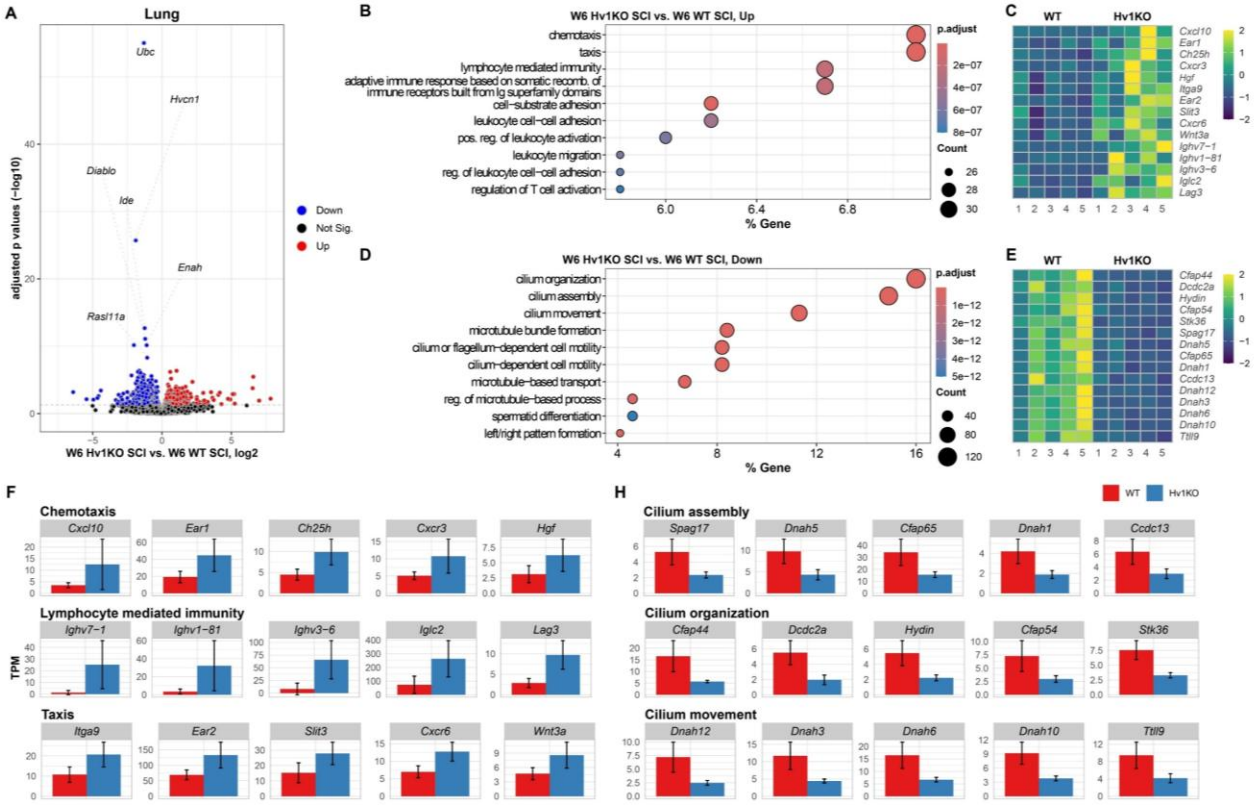

Figure 12. Hv1 depletion reshapes chronic lung transcriptomic programs in aged mice 6 weeks post-SCI. (A) Differential expression analysis (volcano plot) comparing Hv1 KO/SCI vs. WT/SCI. **(B–E)** Functional enrichment of upregulated (B) and downregulated (D) DEGs, with corresponding heatmaps of representative genes from the top enriched pathways (C, E)**. (F–H)** Expression levels of selected DEGs displayed as bar plots, grouped by functional categories, including chemotaxis, lymphocyte-mediated immunity, and taxis (F), and cilium assembly, cilium organization, and cilium movement (H). n=5 mice/group.

In peripheral spleen tissue, Hv1 ablation significantly modulated persistent immune activation and inflammation. A volcano plot highlighted genetic differences between WT/SCI and KO/SCI groups (Fig. 11A). Pathway analysis (Fig. 11B-E) identified "nuclear division," "chromosome segregation," and "cell chemotaxis" as top upregulated processes in KO/SCI mice, whereas genes related to "adaptive immune response," "immunoglobulin-mediated immunity," "B cell–mediated immunity," and "regulation of GTPase activity" were downregulated. Notable DEGs included *Ankle1*, *Chek1*, *Birc5*, and *Top2a* among upregulated genes, while downregulated genes were mainly immunoglobulin heavy variable genes (*Ighv5-6*, *Ighv5-12*, *Ighv1-62-2*, *Ighv1-5*, *Ighv2-3*). Bar graph visualization confirmed consistent pathway expression shifts across conditions (Fig. 11F). Baseline comparison of aged Hv1 KO and WT mice (KO/Sham vs. WT/Sham) revealed few splenic DEGs (Supplementary Fig. 10A). Upregulated DEGs were mainly associated with "myeloid leukocyte migration" and "chemotaxis" (Supplementary Fig. 10B-C), while downregulated DEGs involved "B cell activation" and "lymphocyte proliferation" (Supplementary Fig. 10D-E). After injury, aged Hv1 KO mice showed mostly downregulated DEGs, with only a few upregulated, contrasting with WT mice (Supplementary Fig. 11A). Upregulated pathways included neutrophil chemotaxis and killing/disruption of other organism's cells (Supplementary Fig. 11B-C), while downregulated pathways involved erythrocyte differentiation, homeostasis, and protein polymerization (Supplementary Fig. 11D-E). Key genes included *Ccl19-ps1* and *Cxcl10* (upregulated) and *Klf1*, *Epb42*, *Dmtn*, and *Ypel4* (downregulated). A previous study reported that chronic SCI leads to a sustained upregulation of tyrosine hydroxylase (TH) in the mouse spleen, resulting in T-cell exhaustion, impaired T-cell function, and immune depression [82]. Consistent with this report, our Western blot analysis showed a 1.8-fold increase in TH expression after SCI (p=0.05, Fig. 13A, Supplementary Fig. 12). Notably, Hv1 deficiency reversed the SCI-induced elevation of TH (p=0.02). There was no significant difference in Hv1 expression between WT/SCI and WT/Sham groups. These findings suggest that Hv1 contributes to the regulation of splenic sympathetic activity after SCI and that Hv1 ablation may prevent SCI-induced T-cell dysfunction and immune dysregulation.

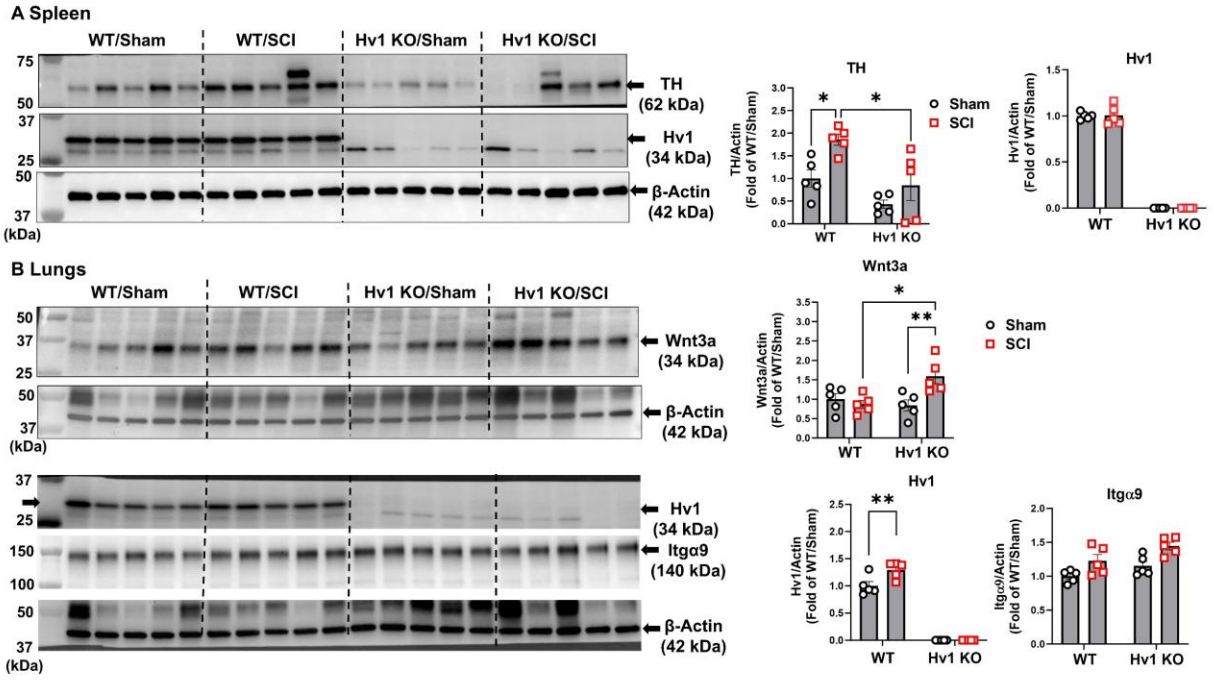

Figure 13. Systemic deletion of Hv1 modifies chronic protein expression profiles in the spleen and lungs of aged mice at 42 days following SCI. (A) Western blot analysis of tyrosine hydroxylase (TH) and Hv1 expression in the spleen was performed, and representative images are shown. (**B**) Western blot analysis was conducted to examine protein expression in lung tissue, and representative bands for Wnt3a, Hv1, and Itgα9 are presented. n=5 mice/group. Protein levels were quantified by densitometry, normalized to β-Actin, and presented as fold change compared to WT/Sham (unedited western blots in Fig. S12). *p<0.05, **p< 0.01. Two-way ANOVA following Tukey's multiple comparisons test.

In lung tissue, Hv1 ablation markedly altered the transcriptomic profile of aged mice after chronic SCI (Fig. 12A). GO analysis showed upregulation of genes involved in chemotaxis and adaptive immunity (Fig. 12B-C) and downregulation of pathways related to cilium organization and motility (Fig. 12D-E). Key upregulated genes included *Cxcl10*, *Cxcr3*, *Itga9*, and *Wnt3a* (Fig. 12C and F), while downregulated genes included *Dcdc2a*, *Hydin*, *Stk36*, and *Spag17* (Fig. 12E and H). Baseline comparison of KO/Sham and WT/Sham lungs revealed significant genotype-dependent transcriptomic differences (Supplementary Fig. 13A). Upregulated genes were associated with "wound healing," "blood coagulation," and "coagulation" (Supplementary Fig. 13B-C), including *Slc4a1*, *Alox15*, *Gp1bb*, and *F10*, while downregulated genes affected only "response to redox state" and included *Npas2* (Supplementary Fig. 13D-E), highlighting the role of the Hv1 channel in aging. SCI in aged Hv1 KO mice induced distinct transcriptomic changes (Supplementary Fig. 14A). Upregulated genes were enriched in "ameboidal-type cell migration," "regulation of neurogenesis," and "regionalization" (e.g., *Lefty1*, *Dll4*, *Kitl*, *Jcad*, *Sema3g*) (Supplementary Fig. 14B-C), while downregulated genes affected "IL-6 production" and "response to bacterial molecules" (e.g., *Spon2*, *Ticam2*, *Tlr1*, *Ptafr*, *Mbp*) (Supplementary Fig. 14D-E). These results show Hv1 ablation drives injury- and genotype-dependent transcriptomic profiles, enhancing chemotactic/ proliferative signaling, suppressing B cell immunity, and modulating erythrocyte, coagulation, and innate immune pathways in lung. Wnt3a signaling has been reported to attenuate motor neuron loss and promote tissue repair and functional recovery after SCI by reducing inflammation and apoptosis [83, 84]. Interestingly, several studies have also shown that Wnt3a decreases alveolar epithelial cell death, supports epithelial regeneration, and improves pulmonary function following lung injury [85, 86]. We compared lung Wnt3a protein expression across injury conditions and genotypes (Fig. 13B, Supplementary Fig. 12). Compared with Sham, Wnt3a expression in the lung was markedly increased after SCI in Hv1 KO mice (p=0.013), whereas no significant change was observed in WT animals. Moreover, following SCI, Wnt3a levels were significantly higher in Hv1 KO mice than in WT mice (p=0.017). Interestingly, SCI also induced a significant increase in Hv1 expression in the lungs compared with Sham mice (p=0.006) (Fig. 13B). Itgα9 has been reported to play a role in neutrophil migration through the human lung [82]. However, we did not detect significant differences in

Itgα9 protein levels between Sham and SCI groups or between WT and Hv1 KO mice. In conclusion, our findings suggest that Hv1 may contribute to the regulation of lung function after SCI through the Wnt3a pathway.

Hv1 inhibition reduces proinflammatory signaling and enhances locomotor recovery in the acutely injured aged mice

To evaluate the therapeutic potential of Hv1 inhibition, we conducted a pilot study in aged (22-month-old) male C57BL/6 mice using 2-GBI, a compound experimentally shown to reduce microglial activation and the production of proinflammatory mediators [56, 57]. Aged mice subjected to SCI received 2-GBI once daily for 7 days via intraperitoneal injection, beginning 30 minutes post-injury. We observed a significant increase in BMS scores at 7 days post-injury in 2-GBI-treated mice (Supplementary Fig. 15A, p=0.004). A significant main effect of Post-injury Day was detected ($F(3, 21) = 5.269$, p=0.007), whereas the effects of Treatment ($F(1, 7) = 4.481$, $p = 0.072$) and the Treatment × Day interaction ($F(3, 21) = 2.202$, $p = 0.118$) were not significant. Western blot analysis showed reduced expression of the innate immune response markers cGAS (p=0.0159) and STING (p=0.0317), as well as the microglia/macrophage marker Iba-1 (p=0.0317), in mice treated with 2-GBI compared with vehicle controls at 7 days after SCI (Supplementary Fig. 15B–C, Supplementary Fig. 16), indicating attenuated neuroinflammation. These findings are consistent with the neuroprotective effects observed in mice with genetic Hv1 deletion. Collectively, these data suggest that the Hv1 inhibitor 2-GBI has beneficial effects on SCI-mediated neuroinflammation and appears to protect against acute SCI in aged animals.

DISCUSSION

Spinal cord injury induces systemic effects across multiple organs, but the molecular changes associated with aging remain largely undefined. Here, we examined the role of the voltage-gated proton channel Hv1 in SCI-induced immune responses in aged mice. Our study is the first to demonstrate that age-related upregulation of Hv1 amplifies both intraspinal injury and peripheral organ dysfunction after SCI. Using aged Hv1 KO mice, we reveal that Hv1 deletion confers broad neuroprotection and systemic benefits - promoting chromatin remodeling and Wnt signaling, suppressing NF-κB-driven inflammation and oxidative stress, and restoring immune balance across the spinal cord, spleen, and lungs. Functionally, loss of Hv1 improved locomotor recovery and reduced tissue damage in aged SCI mice. These findings uncover a previously unrecognized role of Hv1 as an age-dependent regulator of neuro-immune crosstalk and identify it as a potential therapeutic target for improving recovery in elderly SCI patients.

Aging is a critical determinant of SCI, with older individuals showing increased incidence and severity [3, 4]. Our previous work in aged mice demonstrated exacerbated motor and cognitive deficits and worsened tissue damage after SCI compared to young adults [87], consistent with other studies [14, 88]. Despite these observations, mechanisms driving age-related pathology after SCI remain poorly understood. For instance, Zhang et al. [88] reported that middle-aged mice exhibited heightened inflammatory responses, elevated ROS production, and impaired locomotor recovery following SCI, driven in part by enhanced NADPH oxidase (NOX2) activation in macrophages and microglia [14]. These findings suggest that chronic neuroinflammation driven by infiltrating lymphocytes contributes to neurodegeneration and impaired functional recovery in aged subjects. Hv1 is critical for NADPH-dependent ROS generation in microglia and macrophages [28, 29]. It is abundantly expressed across innate immune cells, including neutrophils, macrophages, and lymphocytes [27]. After SCI, its upregulation intensifies neuroinflammation and contributes to secondary tissue injury [34, 36, 38, 40]. In agreement with previous findings [42, 43], we observed a ~40% increase in Hv1 RNA expression in the brain of aged mice, indicating a chronic inflammatory state. Notably, SCI induced a 5-6-fold increase in spinal cord Hv1 expression at 7 days post-injury, sustained through 6 weeks, suggesting that SCI amplifies Hv1 upregulation beyond age-related changes.

Spinal cord RNA-seq revealed distinct transcriptional profiles in aged Hv1 KO vs. WT mice after SCI. Under sham conditions, Hv1 KO mice exhibited downregulation of immune activation and inflammatory signaling, including IL-6 and interleukin production, indicating reduced basal inflammation. Following acute SCI, both WT and Hv1 KO mice showed upregulation of immune-related pathways, reflecting robust innate and adaptive immune activation. Notably, Hv1 deletion also promoted neuroprotective pathways, including chromatin remodeling and *Wnt* signaling, supporting axon regeneration, neural repair, and DNA damage repair *via* genes such as *Kdm5a* and *Kdm2a* [89-94]. Downregulation of bioenergetic and metabolic pathways in Hv1 KO mice may limit excessive ROS production and oxidative stress, further mitigating secondary injury [95-98].

Behavioral and histological assessments confirmed that Hv1 ablation improved locomotor recovery and reduced tissue loss after SCI in aged mice. Following chronic SCI, transcriptional changes persisted, with SCI continuing to upregulate immune pathways and

downregulate neurogenesis-related pathways in aged WT mice. Notable DEGs in the upregulated pathways have been found to promote the release of pro-inflammatory cytokines and demyelination after injury, such as *Mmp12* [64, 65], and are essential in the clearance of apoptotic cells, such as *Cd300lf* and *Cd300a* [66]. Previous studies have shown that detecting high levels of *Cd300a* in the serum of patients in the subacute phase (from 30 to 120 days) are associated with a lack of recovery following SCI [68]. Another proinflammatory gene is *Adam8*, which has been often implicated as a promoter of cell migration, chemotaxis, and secretion of inflammatory mediators [69]. Finally, the gene *Lcn2* has been found to be highly expressed in astrocytes following SCI, facilitating the activation and recruitment of microglia in local neuroinflammation at the injury site [70, 71]. When comparing Hv1 KO/SCI to WT/SCI, only a small number of DEGs were observed, which resulted in only the upregulated DEG showing up on GO analysis, encompassing processes of circadian rhythm, circadian behavior, rhythmic behavior, circadian regulation of gene expression, and positive regulation of T cell proliferation. Circadian rhythms control the daily cycles of gene expression, which in turn regulate key physiological processes involved in the immediate response to injury, such as immune function and inflammation [99, 100]. Preclinical studies show that circadian disruption heightens microglial activation and proinflammatory cytokine production, impairing recovery after CNS injuries, including ischemic brain injury [101], TBI [102], and SCI [103, 104]. In Hv1 KO mice, upregulation of circadian genes at both the transcript and protein levels may alter immune, metabolic, and repair rhythms, potentially promoting post-SCI recovery, consistent with observations from other studies [103, 104]. Thus, Hv1 contributes to age-related worsening of SCI by driving chronic inflammation and secondary tissue damage. Deletion of Hv1 mitigates these effects, promoting tissue repair, modulating immune responses, and facilitating functional recovery in aged mice.

Beyond the local lesion, SCI triggers systemic inflammation and immune suppression that affect peripheral organs such as the spleen and lungs [18, 22, 23, 105, 106]. At 7 days post-SCI, the spleen serves as a major immune reservoir [20, 107]. Splenic monocytes enter circulation and infiltrate the lesion, where they worsen secondary damage *via* pro-inflammatory cytokines (TNF-α, IL-1β, IL-6) and ROS [108-110]. Early monocyte/macrophage infiltration predicts poorer recovery [107], whereas suppressing systemic immunity improves locomotion by reducing neutrophils and retaining splenic monocytes [111]. T cells further exacerbate injury: their activation disrupts the blood–spinal cord barrier through perforin, promoting cytokine infiltration [112]. Blocking T cell recruitment with CXCL10 preserves tissue and function [113]. Aging increases splenic monocyte/macrophage accumulation, reduces autophagy, and skews cytokine production [114]. We therefore investigated the role of Hv1 in modulating splenic responses to SCI in aged mice. Hv1 KO/Sham vs. WT/Sham differences revealed heightened immune activation and proliferation pathways in Hv1-deficient spleens, suggesting a shift toward enhanced immune responsiveness despite aging. Seven days after SCI, RNA-seq confirmed that SCI induced systemic immune activation in WT spleens, with genes promoting proliferation and protein metabolism. Among these, Cdc6 - previously linked to glial proliferation in SCI [115] and poor prognosis in glioma [116] - was upregulated, implicating it in immune cell expansion and inflammatory cascades. Hv1 deletion suppressed this proliferative response, indicating a protective effect. We also found that aging-associated *Isg20*, a marker of immunosenescence [61], was reduced by Hv1 deletion, suggesting preserved immune competence. Furthermore, Hv1 KO enhanced adaptive immune pathways. While SCI suppresses lymphocyte, macrophage, and NK cell activity in young mice [82, 117], our RNA-seq data indicate that Hv1 deletion prevents such dysfunction in aged mice, supporting a beneficial role for Hv1 loss in maintaining immune function after SCI.

Chronic neuroinflammation driven by infiltrating lymphocytes may underlie poor recovery after SCI in aged subjects. Our RNA-seq analysis of spleen at 6 weeks post-SCI reveals a novel chronic response: robust upregulation of ribosomal protein genes, highlighting protein synthesis pathways. To our knowledge, this is the first report of ribosomal gene induction in the spleen at a chronic SCI timepoint, especially in aged animals. Previous studies of splenic gene expression after SCI largely describe immune dysfunction, cytokine signaling, splenic atrophy, or immunosuppression-not ribosomal upregulation, which has otherwise been observed in chronic infection, genetic models, or systemic stress [74, 75, 118]. Notably, loss of *miR-132/212* in splenic CD4(+) T cells during chronic infection drives increased RP gene expression [119], suggesting parallels to chronic SCI. These findings may reveal new mechanisms of systemic immune remodeling and therapeutic targets for persistent inflammation after injury. Hv1 ablation further shaped splenic responses. PLS-DA showed distinct profiles separating Hv1 KO/SCI from WT/SCI, with Hv1 KO changes forming a near-mirror image of WT/SCI. Hv1 deletion enhanced pathways linked to immune cell proliferation and migration, potentially counteracting SCI-induced immunosuppression. Normally, elevated splenic norepinephrine within 2 weeks of SCI drives immune cell apoptosis and reduced antibody production

[18]. In Hv1 KO mice, upregulated proliferative pathways may restore immune cell pools, enabling migration to injury sites, dampening inflammation, and improving recovery [120, 121]. Together, these results highlight splenic vulnerability to SCI and suggest that maladaptive immune suppression may contribute to worse outcomes in aging.

The lungs are highly vulnerable to secondary inflammation after SCI [21]. Pulmonary complications are the leading causes of morbidity and mortality in SCI patients [122, 123], partly due to SCI-induced systemic immune suppression, including reduced circulating leukocytes and immune modulatory genes [21, 124]. Advanced age further increases the risk of recurrent pneumonia [125, 126], driven by elevated inflammatory cytokines [62], cellular senescence, and altered damage-associated molecular patterns [63]. RNAseq of aged mouse lungs following SCI revealed marked transcriptional changes. Seven days after injury, WT mice showed upregulation of chemotaxis, leukocyte migration, and myeloid differentiation pathways, with DEGs (*Retnlg*, *S100a8/a9*, *Cxcr2*, *Trem1*, *Ccr1*) supporting a pro-inflammatory response. Hv1 ablation shifted responses toward adaptive immunity, enhancing T cell activation, leukocyte adhesion, and cell cycle regulation, while suppressing senescence, ROS metabolism, apoptosis, and cytokine signaling. Changes in *Wnt10b*, *Socs1*, *Nos3*, *Acox1*, *Ddit4*, *Bnip3*, and *Ccr1* suggest Hv1 loss dampens lung inflammation and preserves function. Six weeks post-SCI, WT lungs exhibited persistent transcriptomic alterations, with upregulated cilium organization and motility (*Cfap44*, *Cfap43*, *Dnah5*) and downregulated ECM and immune pathways (*Egfl6*, *Col3a1*, *Col5a3*, *Eln*, *Ndnf*), reflecting structural deterioration and ongoing inflammation. Hv1 ablation reversed many effects, boosting chemotaxis, adaptive immunity, and leukocyte activation while reducing ciliary remodeling. Upregulation of *Itga9* and *Wnt3a* highlighted enhanced proliferation and *Wnt*-driven tissue repair. These results highlight the lung's vulnerability to post-SCI inflammation and identify Hv1 as a key driver of immune dysregulation and tissue remodeling in chronic SCI.

In summary, our study demonstrates that SCI triggers transcriptomic changes linked to immune and inflammatory responses in both the spinal cord and peripheral organs (spleen and lung) of aged male mice during the acute and chronic phases of injury. Loss of Hv1 attenuated secondary inflammation, enhanced immune activity, and improved locomotor recovery while reducing tissue damage compared to WT controls, accompanied by transcriptomic and neuronal alterations. These findings reveal potential molecular mechanisms underlying SCI-induced central and peripheral complications in the elderly and highlight the importance of developing therapeutic strategies to mitigate systemic inflammation and improve recovery in this vulnerable population. Hv1 is well-characterized in immune cells such as microglia and peripheral phagocytes, but its expression in non-immune CNS or systemic cells is limited. Endothelial cells and most neurons show minimal Hv1, whereas certain epithelial cells (e.g., airway, gastric, pancreatic) do express it. Therefore, Hv1's effects on peripheral organs are likely driven primarily by immune modulation, though direct roles in Hv1-expressing epithelial cells cannot be excluded. This study has limitations. We used only male mice to limit the number of aged animals required and to avoid confounds across experimental paradigms. The present findings may not apply to aged females, given known sex differences in immune aging and SCI outcomes. Hv1-related sex differences in SCI pathology have not been reported and warrant future investigation. The 2-GBI Hv1-inhibition experiment lasted only 7 days and assessed short-term outcomes, making it difficult to infer effects on chronic SCI reflected in the 6-week transcriptomic data. Future studies are needed to evaluate long-term therapeutic potential. Whole-tissue profiling also limited the resolution of region-specific structure-function relationships. Nonetheless, the data provide a broad view of Hv1's impact on SCI-induced systemic complications.

Acknowledgements

This study was supported by the National Institute of Neurological Disorders and Stroke (NINDS) R01 NS110825 (JW) and both the NINDS and the National Institute on Aging R01 NS094527 (JW) and R01 AG 077541 (JW). We would like to thank Mr. Hui Li for his assistance with animal care and tissue sectioning.

Author Contributions

J.W. conceived the project and designed the experiments. Z.W., Y.L., and Z.L. performed experiments and sample processing. Z.W., Y.L., H.L., and Z.L. performed data curation, formal analysis, investigation, and visualization. L-J W. provided the Hv1 KO mice, project discussion, and manuscript revision. Z.W., Y.L., and J.W. wrote the manuscript. All authors approved the final version of the manuscript.

Conflict of Interest

The authors declare no competing financial interest.

Data Availability Statement

All data needed to evaluate the conclusions in the paper are present in the paper and/or the Supplementary Materials. All RNA-seq data were deposited in the Gene Expression Omnibus (GEO) under the accession number: GSE 313209 at www.ncbi.nlm.nih.gov/geo/query/acc.cgi?acc=GSE313209.

Supplementary Materials

The Supplementary data can be found online at: www.aginganddisease.org/EN/10.14336/AD.2025.1122.

References

[1] Ahuja CS, Nori S, Tetreault L, Wilson J, Kwon B, Harrop J, et al. (2017). Traumatic Spinal Cord Injury-Repair and Regeneration. Neurosurgery, 80:S9-S22.

[2] Aarabi B, Albrecht JS, Simard JM, Chryssikos T, Schwartzbauer G, Sansur CA, et al. (2021). Trends in Demographics and Markers of Injury Severity in Traumatic Cervical Spinal Cord Injury. J Neurotrauma, 38:756-764.

[3] Qin H, Diao Y, Hao M, Wang Z, Xie M, Hu X, et al. (2024). Analysis and comparison of the trends in burden of spinal cord injury in China and worldwide from 1990 to 2021: an analysis of the global burden of disease study 2021. Front Public Health, 12:1517871.

[4] Ding W, Hu S, Wang P, Kang H, Peng R, Dong Y, et al. (2022). Spinal Cord Injury: The Global Incidence, Prevalence, and Disability From the Global Burden of Disease Study 2019. Spine (Phila Pa 1976), 47:1532-1540.

[5] Xing L, Bao Y, Wang B, Shi M, Wei Y, Huang X, et al. (2023). Falls caused by balance disorders in the elderly with multiple systems involved: Pathogenic mechanisms and treatment strategies. Front Neurol, 14:1128092.

[6] Engel-Haber E, Zeilig G, Haber S, Worobey L, Kirshblum S (2020). The effect of age and injury severity on clinical prediction rules for ambulation among individuals with spinal cord injury. Spine J, 20:1666-1675.

[7] Brouwers E, Meent HV, Curt A, Maier DD, Abel RF, Weidner N, et al. (2020). Recovery after traumatic thoracic- and lumbar spinal cord injury: the neurological level of injury matters. Spinal Cord, 58:980-987.

[8] Oleson CV, Marino RJ, Leiby BE, Ditunno JF (2016). Influence of Age Alone, and Age Combined With Pinprick, on Recovery of Walking Function in Motor Complete, Sensory Incomplete Spinal Cord Injury. Arch Phys Med Rehabil, 97:1635-1641.

[9] Elsamadicy AA, Serrato P, Belkasim S, Ghanekar SD, Khalid SI, Lo SL, et al. (2025). Impact of patient age on morbidity and mortality in adults with acute traumatic cervical spinal cord injury: An ACS trauma quality programs database study. Clin Neurol Neurosurg, 249:108740.

[10] Stewart AN, Jones LAT, Gensel JC (2022). Improving translatability of spinal cord injury research by including age as a demographic variable. Front Cell Neurosci, 16:1017153.

[11] Gwak YS, Hains BC, Johnson KM, Hulsebosch CE (2004). Locomotor recovery and mechanical hyperalgesia following spinal cord injury depend on age at time of injury in rat. Neurosci Lett, 362:232-235.

[12] Siegenthaler MM, Ammon DL, Keirstead HS (2008). Myelin pathogenesis and functional deficits following SCI are age-associated. Exp Neurol, 213:363-371.

[13] Hooshmand MJ, Galvan MD, Partida E, Anderson AJ (2014). Characterization of recovery, repair, and inflammatory processes following contusion spinal cord injury in old female rats: is age a limitation? Immun Ageing, 11:15.

[14] Zhang B, Bailey WM, McVicar AL, Gensel JC (2016). Age increases reactive oxygen species production in macrophages and potentiates oxidative damage after spinal cord injury. Neurobiol Aging, 47:157-167.

[15] Zhang B, Bailey WM, McVicar AL, Stewart AN, Veldhorst AK, Gensel JC (2019). Reducing age-dependent monocyte-derived macrophage activation contributes to the therapeutic efficacy of NADPH oxidase inhibition in spinal cord injury. Brain Behav Immun, 76:139-150.

[16] DeVivo MJ, Shewchuk RM, Stover SL, Black KJ, Go BK (1992). A cross-sectional study of the relationship between age and current health status for persons with spinal cord injuries. Paraplegia, 30:820-827.

[17] Pruss H, Tedeschi A, Thiriot A, Lynch L, Loughhead SM, Stutte S, et al. (2017). Spinal cord injury-induced immunodeficiency is mediated by a sympathetic-neuroendocrine adrenal reflex. Nat Neurosci, 20:1549-1559.

[18] Lucin KM, Sanders VM, Jones TB, Malarkey WB, Popovich PG (2007). Impaired antibody synthesis after spinal cord injury is level dependent and is due to sympathetic nervous system dysregulation. Exp Neurol, 207:75-84.

[19] Riegger T, Conrad S, Liu K, Schluesener HJ, Adibzahdeh M, Schwab JM (2007). Spinal cord injury-induced immune depression syndrome (SCI-IDS). Eur J Neurosci, 25:1743-1747.

[20] Noble BT, Brennan FH, Popovich PG (2018). The spleen as a neuroimmune interface after spinal cord injury. J Neuroimmunol, 321:1-11.

[21] Berk BC, Pereira A, Vizcarra VS, Proschel C, Hsu CG (2024). Spinal cord injury enhances lung inflammation and exacerbates immune response following exposure to LPS. Front Immunol, 15:1483402.

[22] Cardozo CP (2007). Respiratory complications of spinal cord injury. J Spinal Cord Med, 30:307-308.

[23] Gris D, Hamilton EF, Weaver LC (2008). The systemic inflammatory response after spinal cord injury damages lungs and kidneys. Exp Neurol, 211:259-270.

[24] Kopp MA, Watzlawick R, Martus P, Failli V, Finkenstaedt FW, Chen Y, et al. (2017). Long-term functional outcome in patients with acquired infections after acute spinal cord injury. Neurology, 88:892-900.

[25] Failli V, Kopp MA, Gericke C, Martus P, Klingbeil S, Brommer B, et al. (2012). Functional neurological recovery after spinal cord injury is impaired in patients with infections. Brain, 135:3238-3250.
[26] DeCoursey TE (2013). Voltage-gated proton channels: molecular biology, physiology, and pathophysiology of the H(V) family. Physiol Rev, 93:599-652.
[27] He J, Ritzel RM, Wu J (2021). Functions and Mechanisms of the Voltage-Gated Proton Channel Hv1 in Brain and Spinal Cord Injury. Front Cell Neurosci, 15:662971.
[28] Ramsey IS, Ruchti E, Kaczmarek JS, Clapham DE (2009). Hv1 proton channels are required for high-level NADPH oxidase-dependent superoxide production during the phagocyte respiratory burst. Proc Natl Acad Sci U S A, 106:7642-7647.
[29] Wu LJ, Wu G, Akhavan Sharif MR, Baker A, Jia Y, Fahey FH, et al. (2012). The voltage-gated proton channel Hv1 enhances brain damage from ischemic stroke. Nat Neurosci, 15:565-573.
[30] Tian DS, Li CY, Qin C, Murugan M, Wu LJ, Liu JL (2016). Deficiency in the voltage-gated proton channel Hv1 increases M2 polarization of microglia and attenuates brain damage from photothrombotic ischemic stroke. J Neurochem, 139:96-105.
[31] Liu J, Tian D, Murugan M, Eyo UB, Dreyfus CF, Wang W, et al. (2015). Microglial Hv1 proton channel promotes cuprizone-induced demyelination through oxidative damage. J Neurochem, 135:347-356.
[32] Chen M, Yang LL, Hu ZW, Qin C, Zhou LQ, Duan YL, et al. (2020). Deficiency of microglial Hv1 channel is associated with activation of autophagic pathway and ROS production in LPC-induced demyelination mouse model. J Neuroinflammation, 17:333.
[33] Neal ML, Beier EE, Hossain MM, Boyle A, Zheng J, Kim C, et al. (2023). Voltage-Gated Proton Channel Hv1 Regulates Neuroinflammation and Dopaminergic Neurodegeneration in Parkinson's Disease Models. Antioxidants (Basel), 12.
[34] Li Y, Ritzel RM, He J, Cao T, Sabirzhanov B, Li H, et al. (2021). The voltage-gated proton channel Hv1 plays a detrimental role in contusion spinal cord injury via extracellular acidosis-mediated neuroinflammation. Brain Behav Immun, 91:267-283.
[35] Ritzel RM, He J, Li Y, Cao T, Khan N, Shim B, et al. (2021). Proton extrusion during oxidative burst in microglia exacerbates pathological acidosis following traumatic brain injury. Glia, 69:746-764.
[36] Murugan M, Zheng J, Wu G, Mogilevsky R, Zheng X, Hu P, et al. (2020). The voltage-gated proton channel Hv1 contributes to neuronal injury and motor deficits in a mouse model of spinal cord injury. Mol Brain, 13:143.
[37] Li X, Yu Z, Zong W, Chen P, Li J, Wang M, et al. (2020). Deficiency of the microglial Hv1 proton channel attenuates neuronal pyroptosis and inhibits inflammatory reaction after spinal cord injury. J Neuroinflammation, 17:263.
[38] Li X, Liu R, Yu Z, He D, Zong W, Wang M, et al. (2020). Microglial Hv1 exacerbates secondary damage after spinal cord injury in mice. Biochem Biophys Res Commun.
[39] Ritzel RM, Li Y, Jiao Y, Lei Z, Doran SJ, He J, et al. (2023). Brain injury accelerates the onset of a reversible age-related microglial phenotype associated with inflammatory neurodegeneration. Sci Adv, 9:eadd1101.
[40] Li Y, Xie Y, Liu R, Wang Z, Chen P, Wang M, et al. (2023). Knockout of microglial Hv1 proton channel reduces neurotoxic A1 astrocytes and neuronal damage via the ROS/STAT3 pathway after spinal cord injury. Glia, 71:2418-2436.
[41] Liu X, Lei Z, Gilhooly D, He J, Li Y, Ritzel RM, et al. (2023). Traumatic brain injury-induced inflammatory changes in the olfactory bulb disrupt neuronal networks leading to olfactory dysfunction. Brain Behav Immun, 114:22-45.
[42] Zhang ZJ, Zheng XX, Zhang XY, Zhang Y, Huang BY, Luo T (2020). Aging alters Hv1-mediated microglial polarization and enhances neuroinflammation after peripheral surgery. CNS Neurosci Ther, 26:374-384.
[43] Kawai T, Takao K, Akter S, Abe M, Sakimura K, Miyakawa T, et al. (2021). Heterogeneity of microglial proton channel in different brain regions and its relationship with aging. J Neurochem, 157:624-641.
[44] Matyas JJ, O'Driscoll CM, Yu L, Coll-Miro M, Daugherty S, Renn CL, et al. (2017). Truncated TrkB.T1-Mediated Astrocyte Dysfunction Contributes to Impaired Motor Function and Neuropathic Pain after Spinal Cord Injury. J Neurosci, 37:3956-3971.
[45] Basso DM, Fisher LC, Anderson AJ, Jakeman LB, McTigue DM, Popovich PG (2006). Basso Mouse Scale for locomotion detects differences in recovery after spinal cord injury in five common mouse strains. J Neurotrauma, 23:635-659.
[46] Tashiro S, Nakamura M, Okano H (2017). The prospects of regenerative medicine combined with rehabilitative approaches for chronic spinal cord injury animal models. Neural Regen Res, 12:43-46.
[47] Metz GA, Whishaw IQ (2009). The ladder rung walking task: a scoring system and its practical application. J Vis Exp.
[48] Li Y, Lei Z, Ritzel RM, He J, Li H, Choi HMC, et al. (2022). Impairment of autophagy after spinal cord injury potentiates neuroinflammation and motor function deficit in mice. Theranostics, 12:5364-5388.
[49] Dobin A, Davis CA, Schlesinger F, Drenkow J, Zaleski C, Jha S, et al. (2013). STAR: ultrafast universal RNA-seq aligner. Bioinformatics, 29:15-21.
[50] Li B, Dewey CN (2011). RSEM: accurate transcript quantification from RNA-Seq data with or without a reference genome. BMC Bioinformatics, 12:323.
[51] Love MI, Huber W, Anders S (2014). Moderated estimation of fold change and dispersion for RNA-seq data with DESeq2. Genome Biol, 15:550.
[52] Wu T, Hu E, Xu S, Chen M, Guo P, Dai Z, et al. (2021). clusterProfiler 4.0: A universal enrichment tool for interpreting omics data. Innovation (Camb), 2:100141.
[53] Hong L, Singh V, Wulff H, Tombola F (2015). Interrogation of the intersubunit interface of the open

Hv1 proton channel with a probe of allosteric coupling. Sci Rep, 5:14077.
[54] Hong L, Kim IH, Tombola F (2014). Molecular determinants of Hv1 proton channel inhibition by guanidine derivatives. Proc Natl Acad Sci U S A, 111:9971-9976.
[55] Gianti E, Delemotte L, Klein ML, Carnevale V (2016). On the role of water density fluctuations in the inhibition of a proton channel. Proc Natl Acad Sci U S A, 113:E8359-E8368.
[56] Sun L, Wang X, Guan S, Chi L, Liang M, Lu X, et al. (2024). Inhibition of voltage-gated Hv1 alleviates LPS-induced neuroinflammation via regulation of microglial metabolic reprogramming. Int Immunopharmacol, 127:111361.
[57] Hernandez-Espinosa DR, Gale JR, Scrabis MG, Aizenman E (2023). Microglial reprogramming by Hv1 antagonism protects neurons from inflammatory and glutamate toxicity. J Neurochem, 165:29-54.
[58] Li Y, Uzun C, Islam ST, Krishnamachary B, Lee H, Wang Z, et al. (2025). Age-dependent Transcriptional and Circuit Alterations in the brain Underlie Post-Anesthesia Neurobehavioral Dysfunction. Aging Dis.
[59] Wulf MJ, Tom VJ (2023). Consequences of spinal cord injury on the sympathetic nervous system. Front Cell Neurosci, 17:999253.
[60] DiSabato DJ, Marion CM, Mifflin KA, Alfredo AN, Rodgers KA, Kigerl KA, et al. (2024). System failure: Systemic inflammation following spinal cord injury. Eur J Immunol, 54:e2250274.
[61] Zheng Y, Liu X, Le W, Xie L, Li H, Wen W, et al. (2020). A human circulating immune cell landscape in aging and COVID-19. Protein Cell, 11:740-770.
[62] Huffman EE, Dong BE, Clarke HA, Young LEA, Gentry MS, Allison DB, et al. (2023). Cervical spinal cord injury leads to injury and altered metabolism in the lungs. Brain Commun, 5:fcad091.
[63] Rashid K, Sundar IK, Gerloff J, Li D, Rahman I (2018). Lung cellular senescence is independent of aging in a mouse model of COPD/emphysema. Sci Rep, 8:9023.
[64] Wells JE, Rice TK, Nuttall RK, Edwards DR, Zekki H, Rivest S, et al. (2003). An adverse role for matrix metalloproteinase 12 after spinal cord injury in mice. J Neurosci, 23:10107-10115.
[65] Chelluboina B, Nalamolu KR, Klopfenstein JD, Pinson DM, Wang DZ, Vemuganti R, et al. (2018). MMP-12, a Promising Therapeutic Target for Neurological Diseases. Mol Neurobiol, 55:1405-1409.
[66] Lee H, Nakahashi-Oda C, Lyu W, Tanaka M, Rai A, Muramoto Y, et al. (2025). Inhibitory immunoreceptors CD300a and CD300lf cooperate to regulate mast cell activation. J Immunol, 214:325-334.
[67] Nakahashi-Oda C, Fujiyama S, Nakazawa Y, Kanemaru K, Wang Y, Lyu W, et al. (2021). CD300a blockade enhances efferocytosis by infiltrating myeloid cells and ameliorates neuronal deficit after ischemic stroke. Sci Immunol, 6:eabe7915.
[68] Garcia-Ovejero D, Beyerer E, Mach O, Leister I, Strowitzki M, Wutte C, et al. (2024). Untargeted blood serum proteomics identifies novel proteins related to neurological recovery after human spinal cord injury. J Transl Med, 22:666.
[69] Qian Z, Li R, Zhao T, Xie K, Li P, Li G, et al. (2024). Blockade of the ADAM8-Fra-1 complex attenuates neuroinflammation by suppressing the Map3k4/MAPKs axis after spinal cord injury. Cell Mol Biol Lett, 29:75.
[70] Tan Q, Zhang C, Rao X, Wan W, Lin W, Huang S, et al. (2024). The interaction of lipocalin-2 and astrocytes in neuroinflammation: mechanisms and therapeutic application. Front Immunol, 15:1358719.
[71] Wang X, Zhu Z, Zhang Z, Liang Z, Li K, Ma Y, et al. (2024). Astrocyte-derived lipocalin 2 promotes inflammation and scarring after spinal cord injury by activating SMAD in mice. Exp Neurol, 380:114915.
[72] Kim HJ, Jung JI, Kim Y, Lee JS, Yoon YW, Kim J (2010). Loss of hsp70.1 Decreases Functional Motor Recovery after Spinal Cord Injury in Mice. Korean J Physiol Pharmacol, 14:157-161.
[73] Roder K, Werdich AA, Li W, Liu M, Kim TY, Organ-Darling LE, et al. (2014). RING finger protein RNF207, a novel regulator of cardiac excitation. J Biol Chem, 289:33730-33740.
[74] Moon Y (2014). Ribosomal alteration-derived signals for cytokine induction in mucosal and systemic inflammation: noncanonical pathways by ribosomal inactivation. Mediators Inflamm, 2014:708193.
[75] Jiao L, Liu Y, Yu XY, Pan X, Zhang Y, Tu J, et al. (2023). Ribosome biogenesis in disease: new players and therapeutic targets. Signal Transduct Target Ther, 8:15.
[76] Chen G, Fang X, Yu M (2015). Regulation of gene expression in rats with spinal cord injury based on microarray data. Mol Med Rep, 12:2465-2472.
[77] Diaz-Munoz MD, Bell SE, Fairfax K, Monzon-Casanova E, Cunningham AF, Gonzalez-Porta M, et al. (2015). The RNA-binding protein HuR is essential for the B cell antibody response. Nat Immunol, 16:415-425.
[78] Antony D, Brunner HG, Schmidts M (2021). Ciliary Dyneins and Dynein Related Ciliopathies. Cells, 10.
[79] Andrews KL, Nettesheim P, Asai DJ, Ostrowski LE (1996). Identification of seven rat axonemal dynein heavy chain genes: expression during ciliated cell differentiation. Mol Biol Cell, 7:71-79.
[80] Onursal C, Dick E, Angelidis I, Schiller HB, Staab-Weijnitz CA (2021). Collagen Biosynthesis, Processing, and Maturation in Lung Ageing. Front Med (Lausanne), 8:593874.
[81] Tsukui T, Sun KH, Wetter JB, Wilson-Kanamori JR, Hazelwood LA, Henderson NC, et al. (2020). Collagen-producing lung cell atlas identifies multiple subsets with distinct localization and relevance to fibrosis. Nat Commun, 11:1920.
[82] Zha J, Smith A, Andreansky S, Bracchi-Ricard V, Bethea JR (2014). Chronic thoracic spinal cord injury impairs CD8+ T-cell function by up-regulating programmed cell death-1 expression. J Neuroinflammation, 11:65.
[83] Gao K, Niu J, Dang X (2020). Wnt-3a improves functional recovery through autophagy activation via inhibiting the mTOR signaling pathway after spinal cord injury. Neurosci Lett, 737:135305.

[84] Gao K, Shao W, Wei T, Yan Z, Li N, Lv C (2024). Wnt-3a improves functional recovery after spinal cord injury by regulating the inflammatory and apoptotic response in rats via wnt/beta-catenin signaling pathway. Brain Res, 1822:148637.

[85] Gao L, Sun Y, Zhang X, Ma D, Xie A, Wang E, et al. (2023). Wnt3a-Loaded Extracellular Vesicles Promote Alveolar Epithelial Regeneration after Lung Injury. Adv Sci (Weinh), 10:e2206606.

[86] Guo Y, Mishra A, Weng T, Chintagari NR, Wang Y, Zhao C, et al. (2014). Wnt3a mitigates acute lung injury by reducing P2X7 receptor-mediated alveolar epithelial type I cell death. Cell Death Dis, 5:e1286.

[87] Lei Z, Ritzel RM, Li Y, Li H, Faden AI, Wu J (2024). Old age alters inflammation and autophagy signaling in the brain, leading to exacerbated neurological outcomes after spinal cord injury in male mice. Brain Behav Immun, 120:439-451.

[88] Zhang B, Bailey WM, Braun KJ, Gensel JC (2015). Age decreases macrophage IL-10 expression: Implications for functional recovery and tissue repair in spinal cord injury. Exp Neurol, 273:83-91.

[89] Li HW, Zhang HH (2024). The Protein Acetylation after Traumatic Spinal Cord Injury: Mechanisms and Therapeutic Opportunities. Int J Med Sci, 21:725-731.

[90] Wong JK, Zou H (2014). Reshaping the chromatin landscape after spinal cord injury. Front Biol (Beijing), 9:356-366.

[91] Kataria A, Tyagi S (2023). Domain architecture and protein-protein interactions regulate KDM5A recruitment to the chromatin. Epigenetics, 18:2268813.

[92] Liu L, Liu J, Lin Q (2021). Histone demethylase KDM2A: Biological functions and clinical values (Review). Exp Ther Med, 22:723.

[93] Cheng P, Liao HY, Zhang HH (2022). The role of Wnt/mTOR signaling in spinal cord injury. J Clin Orthop Trauma, 25:101760.

[94] Li K, Chen Z, Chang X, Xue R, Wang H, Guo W (2024). Wnt signaling pathway in spinal cord injury: from mechanisms to potential applications. Front Mol Neurosci, 17:1427054.

[95] Liu C, Liu Y, Ma B, Zhou M, Zhao X, Fu X, et al. (2022). Mitochondrial regulatory mechanisms in spinal cord injury: A narrative review. Medicine (Baltimore), 101:e31930.

[96] Jia Z, Zhu H, Li J, Wang X, Misra H, Li Y (2012). Oxidative stress in spinal cord injury and antioxidant-based intervention. Spinal Cord, 50:264-274.

[97] McEwen ML, Sullivan PG, Rabchevsky AG, Springer JE (2011). Targeting mitochondrial function for the treatment of acute spinal cord injury. Neurotherapeutics, 8:168-179.

[98] Xing Y, Xiao YZ, Zhao M, Zhou JJ, Zhao K, Xiao CL (2025). The role of oxidative stress in spinal cord ischemia reperfusion injury: mechanisms and therapeutic implications. Front Cell Neurosci, 19:1590493.

[99] Durgan DJ, Young ME (2010). The cardiomyocyte circadian clock: emerging roles in health and disease. Circ Res, 106:647-658.

[100] Xu X, Wang J, Chen G (2023). Circadian cycle and neuroinflammation. Open Life Sci, 18:20220712.

[101] Fonken LK, Bedrosian TA, Zhang N, Weil ZM, DeVries AC, Nelson RJ (2019). Dim light at night impairs recovery from global cerebral ischemia. Exp Neurol, 317:100-109.

[102] Darmanto AG, Jan JS, Yen TL, Huang SW, Teng RD, Wang JY, et al. (2024). Targeting Circadian Protein Rev-erbalpha to Alleviate Inflammation, Oxidative Stress, and Enhance Functional Recovery Following Brain Trauma. Antioxidants (Basel), 13.

[103] Gaudet AD, Fonken LK, Ayala MT, Bateman EM, Schleicher WE, Smith EJ, et al. (2018). Spinal Cord Injury in Rats Disrupts the Circadian System. eNeuro, 5.

[104] Gaudet AD, Fonken LK, Ayala MT, Dangelo HM, Smith EJ, Bateman EM, et al. (2019). Spinal Cord Injury in Rats Dysregulates Diurnal Rhythms of Fecal Output and Liver Metabolic Indicators. J Neurotrauma, 36:1923-1934.

[105] Sun X, Jones ZB, Chen XM, Zhou L, So KF, Ren Y (2016). Multiple organ dysfunction and systemic inflammation after spinal cord injury: a complex relationship. J Neuroinflammation, 13:260.

[106] Zhang Y, Guan Z, Reader B, Shawler T, Mandrekar-Colucci S, Huang K, et al. (2013). Autonomic dysreflexia causes chronic immune suppression after spinal cord injury. J Neurosci, 33:12970-12981.

[107] Blomster LV, Brennan FH, Lao HW, Harle DW, Harvey AR, Ruitenberg MJ (2013). Mobilisation of the splenic monocyte reservoir and peripheral CX(3)CR1 deficiency adversely affects recovery from spinal cord injury. Exp Neurol, 247:226-240.

[108] Nguyen HX, O'Barr TJ, Anderson AJ (2007). Polymorphonuclear leukocytes promote neurotoxicity through release of matrix metalloproteinases, reactive oxygen species, and TNF-alpha. J Neurochem, 102:900-912.

[109] Cai Y, Lin Z, Shen X, Li M, Xing L, Yang T, et al. (2025). Effect of microglial Pd1 on glial scar formation after spinal cord injury in mice. J Biol Chem, 301:108489.

[110] Milich LM, Ryan CB, Lee JK (2019). The origin, fate, and contribution of macrophages to spinal cord injury pathology. Acta Neuropathol, 137:785-797.

[111] Ruppert KA, Nguyen TT, Prabhakara KS, Toledano Furman NE, Srivastava AK, Harting MT, et al. (2018). Human Mesenchymal Stromal Cell-Derived Extracellular Vesicles Modify Microglial Response and Improve Clinical Outcomes in Experimental Spinal Cord Injury. Sci Rep, 8:480.

[112] Liu Z, Zhang H, Xia H, Wang B, Zhang R, Zeng Q, et al. (2019). CD8 T cell-derived perforin aggravates secondary spinal cord injury through destroying the blood-spinal cord barrier. Biochem Biophys Res Commun, 512:367-372.

[113] Gonzalez R, Glaser J, Liu MT, Lane TE, Keirstead HS (2003). Reducing inflammation decreases secondary degeneration and functional deficit after spinal cord injury. Exp Neurol, 184:456-463.

[114] Stranks AJ, Hansen AL, Panse I, Mortensen M, Ferguson DJ, Puleston DJ, et al. (2015). Autophagy Controls Acquisition of Aging Features in Macrophages. J Innate Immun, 7:375-391.

[115] Chen C, Lu J, Yu Q, Xiao JR, Wei HF, Song XJ, et al. (2016). Expression of CDc6 after acute spinal cord injury in adult rats. Neuropeptides, 56:59-67.

[116] Wang F, Zhao F, Zhang L, Xiong L, Mao Q, Liu Y, et al. (2022). CDC6 is a prognostic biomarker and correlated with immune infiltrates in glioma. Mol Cancer, 21:153.

[117] Oropallo MA, Held KS, Goenka R, Ahmad SA, O'Neill PJ, Steward O, et al. (2012). Chronic spinal cord injury impairs primary antibody responses but spares existing humoral immunity in mice. J Immunol, 188:5257-5266.

[118] Person JM, Welch BA, Spann RA, Harris KK, Pride Y, Tucci MA, et al. (2020). Immuno-hematologic parameters following rodent spinal cord contusion are negatively influenced by high-fat diet consumption. J Neuroimmunol, 343:577226.

[119] Hewitson JP, Shah KM, Brown N, Grevitt P, Hain S, Newling K, et al. (2019). miR-132 suppresses transcription of ribosomal proteins to promote protective Th1 immunity. EMBO Rep, 20.

[120] Li Y, Zhang C, Li Z, Bai F, Jing Y, Ke H, et al. (2024). Nicotinamide Riboside Regulates Chemotaxis to Decrease Inflammation and Ameliorate Functional Recovery Following Spinal Cord Injury in Mice. Curr Issues Mol Biol, 46:1291-1307.

[121] Li L, Ni L, Heary RF, Elkabes S (2020). Astroglial TLR9 antagonism promotes chemotaxis and alternative activation of macrophages via modulation of astrocyte-derived signals: implications for spinal cord injury. J Neuroinflammation, 17:73.

[122] Urdaneta F, Layon AJ (2003). Respiratory complications in patients with traumatic cervical spine injuries: case report and review of the literature. J Clin Anesth, 15:398-405.

[123] Jackson AB, Groomes TE (1994). Incidence of respiratory complications following spinal cord injury. Arch Phys Med Rehabil, 75:270-275.

[124] Mifflin KA, Brennan FH, Guan Z, Kigerl KA, Filous AR, Mo X, et al. (2022). Spinal Cord Injury Impairs Lung Immunity in Mice. J Immunol, 209:157-170.

[125] Mueller G, Berlowitz DJ, Raab AM, Postma K, Gobets D, Huber B, et al. (2024). Incidence and Risk Factors of Pneumonia in Individuals With Acute Spinal Cord Injury: A Multi-national, Multi-center, Prospective Cohort Study. Arch Phys Med Rehabil, 105:884-891.

[126] Garshick E, Kelley A, Cohen SA, Garrison A, Tun CG, Gagnon D, et al. (2005). A prospective assessment of mortality in chronic spinal cord injury. Spinal Cord, 43:408-416.